

Direen, N.G., Cohen, B.E. , Maas, R., Frey, F.A., Whittaker, J.M., Coffin, M.F., Meffre, S., Halpin, J.A. and Crawford, A.J. (2017) Naturaliste plateau: constraints on the timing and evolution of the Kerguelen Large Igneous Province and its role in Gondwana breakup. *Australian Journal of Earth Sciences*, 64(7), pp. 851-869. (doi:[10.1080/08120099.2017.1367326](https://doi.org/10.1080/08120099.2017.1367326))

This is the author's final accepted version.

There may be differences between this version and the published version. You are advised to consult the publisher's version if you wish to cite from it.

<http://eprints.gla.ac.uk/145758/>

Deposited on: 06 September 2017

Enlighten – Research publications by members of the University of Glasgow  
<http://eprints.gla.ac.uk>



# **Naturaliste Plateau: Constraints on the Timing and Evolution of the Kerguelen Large Igneous Province and its Role in Gondwana Breakup**

Journal:	<i>Australian Journal of Earth Sciences</i>
Manuscript ID	TAJE-RES-2017-0023.R1
Manuscript Type:	Research Paper
Date Submitted by the Author:	07-Aug-2017
Complete List of Authors:	Direen, Nicholas; University of Tasmania, School of Physical Sciences Cohen, Benjamin; Scottish Universities Environmental Research Centre Maas, R; University of Melbourne, School of Earth Sciences Frey, Frederick; Massachusetts Institute of Technology, Earth, Atmosphere and Planetary Sciences Whittaker, Joanne; University of Tasmania Institute for Marine and Antarctic Studies Coffin, Millard; University of Tasmania, Institute for Marine and Antarctic Studies Meffre, Sebastien; University of Tasmania, Earth Sciences Halpin, Jacqueline; University of Tasmania, CODES Crawford, A; University of Tasmania, CODES ARC Centre of Excellence
Keywords:	Naturaliste Plateau, Kerguelen Plume, Gondwanaland breakup, geochronology, geochemistry, Tibet, Wallaby Plateau, Indian Ocean, marine geology

1  
2  
3  
4  
5  
6  
7  
8  
9  
10  
11  
12  
13  
14  
15  
16  
17  
18  
19  
20  
21  
22  
23  
24  
25  
26  
27  
28  
29  
30  
31  
32  
33  
34  
35  
36  
37  
38  
39  
40  
41  
42  
43  
44  
45  
46  
47  
48  
49  
50  
51  
52  
53  
54  
55  
56  
57  
58  
59  
60



# Naturaliste Plateau: Constraints on the timing and evolution of the Kerguelen Large Igneous Province and its role in Gondwana breakup

N. G. Direen<sup>a, b\*</sup>, B. E. Cohen<sup>c, d</sup>, R. Maas<sup>e</sup>, F. A. Frey<sup>f</sup>, J. M. Whittaker<sup>b</sup>, M. F. Coffin<sup>b, g</sup>, S. Meffre<sup>a, h</sup>, J. A. Halpin<sup>a, b, h</sup> and A. J. Crawford<sup>a, h</sup>.

<sup>a</sup> School of Physical Sciences, University of Tasmania, Private Bag 126, Hobart TAS 7001, Australia

<sup>b</sup> Institute for Marine and Antarctic Studies, University of Tasmania, Private Bag 129, Hobart TAS 7001, Australia

<sup>c</sup> School of Earth Sciences, The University of Queensland, St Lucia QLD 4072, Australia

<sup>d</sup> Scottish Universities Environmental Research Centre, East Kilbride, G75 0QF, UK

<sup>e</sup> School of Earth Sciences, University of Melbourne, Parkville, VIC 3010, Australia

<sup>f</sup> Earth, Atmosphere and Planetary Sciences, Massachusetts Institute of Technology, Cambridge, MA 02139-4307, USA

<sup>g</sup> Woods Hole Oceanographic Institution, Woods Hole, MA 02543-1050, USA

<sup>h</sup> ARC Centre of Excellence in Ore Deposits and School of Physical Sciences, University of Tasmania, Private Bag 126, Hobart TAS 7001, Australia

\*Corresponding author: email [n\\_direen@utas.edu.au](mailto:n_direen@utas.edu.au); cell +1 727-517-6874

Postal address: 2523 Bridgestone Park Ln, Spring TX 77386 USA

Received 17 February 2017; accepted 7 August 2017

Editorial handling: Graziella Caprarelli

## Abstract

Volcanism associated with the Kerguelen Large Igneous Province is found scattered in southwestern Australia (the ca 136 to ca 130 Ma Bunbury Basalts, and ca 124 Ma Wallaby Plateau), India (ca 118 Ma Rajmahal Traps and Cona Basalts), and Tibet (the ca 132 Ma Comei Basalts), but apart from the ~70 000 km<sup>2</sup> Wallaby Plateau, these examples are spatially and volumetrically minor. Here, we report dredge, geochronological, and geochemical results from the ~90 000 km<sup>2</sup> Naturaliste Plateau, located ~170 to ~500 km southwest of Australia. Dredged lavas and intrusive rocks range from mafic to felsic compositions, and prior geophysical analyses indicate these units comprise much of the plateau substrate. <sup>40</sup>Ar/<sup>39</sup>Ar plagioclase ages from mafic units and U–Pb zircon ages from silicic rocks indicate magmatic emplacement from 130.6

$\pm 1.2$  to  $129.4 \pm 1.3$  Ma for mafic rocks, and  $131.8 \pm 3.9$  to  $128.2 \pm 2.3$  Ma for silicic rocks ( $2\sigma$ ). These Cretaceous Naturaliste magmas incorporated a significant component of continental crust, with relatively high  $^{87}\text{Sr}/^{86}\text{Sr}$  (up to 0.78), high  $^{207}\text{Pb}/^{204}\text{Pb}$  ratios (15.5–15.6), low  $^{143}\text{Nd}/^{144}\text{Nd}$  (0.511–0.512), and primitive-mantle normalised Th/Nb of 11.3 and La/Nb of 3.97. These geochemical results are consistent with the plateau being underlain by continental basement, as indicated by prior interpretations of seismic and gravity data, corroborated by dredging of Mesoproterozoic granites and gneisses on the southern plateau flank. The Cretaceous Naturaliste Plateau igneous rocks have signatures indicative of extraction from a depleted mantle, with trace element and isotopic values that overlap with Kerguelen Plateau lavas indicative of crustal contamination. Our chemical and geochronological results therefore indicate the Naturaliste Plateau contains evidence of an extensive igneous event representing some of the earliest voluminous Kerguelen hotspot magmas. Prior work indicates that contemporaneous correlative volcanic sequences underlie the nearby Mentelle Basin, and the Enderby Basin and Princess Elizabeth Trough in the Antarctic. When combined, the igneous rocks in the Naturaliste, Mentelle, Wallaby, Enderby, Princess Elizabeth, Bunbury, and Comei-Cona areas form a 136–124 Ma Large Igneous Province covering  $>244\,000\text{ km}^2$ .

Keywords: Naturaliste Plateau; Kerguelen hotspot; Gondwanaland breakup; geochronology; geochemistry; Tibet, Wallaby Plateau

Introduction

The comparatively well-studied, largely submarine Kerguelen Large Igneous Province (LIP) and its conjugate rifted fragment, Broken Ridge (Mutter & Cande, 1983; Tikku & Cande, 2000), together with its onshore correlatives in southwestern Australia (Frey, McNaughton, Nelson, de Laeter, & Duncan, 1996; Olierook et al., 2016), northeastern India (Coffin et al., 2002; Kent, Pringle, Müller, Saunders, & Ghose, 2002; Kent, Saunders, Kempton, & Ghose, 1997), and Tibet (Zhu et al., 2008, 2009), form the second largest known LIP preserved on Earth (Figure 1a). Geochronologic dating of these LIP fragments, now widely separated by rifting, show varying clusters – an apparently spatially minor early component around 137–130 Ma, exposed onshore in Western Australia (the Bunbury Basalt: Figure 1b; Frey et al., 1996, Olierook et al., 2016); and a volumetrically major cluster, which commenced later, around at 124–118 Ma in the main Kerguelen Plateau (Coffin et al., 2002), and the Wallaby Plateau (Olierook et al., 2015) as well as the smaller volumes in south Asia (Coffin et al., 2002; Zhu et al., 2008, 2009).

The age discrepancy between onset of hotspot volcanism around ca 137 Ma, and major expression of volcanism some 13–19 Ma later, have led to speculation about the possibility of a Kerguelen mantle plume “incubating” beneath the extending Gondwana lithosphere (Coffin et al., 2002; Kent et al., 2002; Kent, Storey, & Saunders, 1992; Zhu et al., 2008). Furthermore, despite the large size of the Kerguelen LIP, it is not currently considered to have played a driving role in breakup of the Gondwana supercontinent, as the voluminous 120–118 Ma Kerguelen eruptions post-date rifting by 10–14 Ma (Coffin & Eldholm, 1992).

There are, however, other rifted fragments of the Kerguelen LIP present in the Indian Ocean basin (Figures 1 and 2), which must be evaluated to fully assess links between the LIP and rifting, and to evaluate the models invoking “plume incubation”. In particular, the  $\sim 90\,000\text{ km}^2$

Naturaliste Plateau, offshore from Western Australia (Figure 1b), has been previously correlated with the Kerguelen LIP based on examination of sparse reconnaissance material (Coffin & Eldholm, 1992; Mahoney et al., 1995; Storey et al., 1992).

In this study, we report the results of further extensive dredging of the Naturaliste Plateau by the R/V *Southern Surveyor* in 2005, in order to investigate the origin of this oceanic feature. We present new geochemical and geochronological data from mafic and felsic igneous rocks dredged from the southern margin of the plateau. We then outline how these new data, together with seismic observations from the Naturaliste Plateau and adjacent Mentelle Basin, indicate the formation of a LIP by Kerguelen hotspot impact into the evolving Australia–Antarctica + India–Madagascar spreading margin.

### Regional setting

The Naturaliste Plateau is a quasi-rectangular ~ 250 by 400 km submarine massif rising ~ 2500 m above the surrounding seafloor to water depths of ~ 1600 m (Figure 1b). It covers ~ 90 000 km<sup>2</sup> and is separated by a deep, ~ 170 km wide trough from the southwest Australian mainland (Figure 1b). The Naturaliste Plateau is related to the adjacent more deeply subsided Mentelle Basin (Figure 1b; Maloney, Sargent, Direen, Hobbs, & Grocke, 2011), which occupies a further ~ 44 000 km<sup>2</sup>. The Naturaliste Plateau and Mentelle Basin are located at the intersection of two rift arms formed during Gondwana breakup (Direen, Borissova, Stagg, Colwell, & Symonds, 2007; Direen, Stagg, Symonds, & Colwell, 2008; Jongsma & Petkovic, 1977; Petkovic, 1975; Powell, Roots, & Veevers, 1988; Royer & Coffin, 1992) (Figure 2). Rifting between India–Madagascar and Australia–Antarctica commenced in the Callovian (ca 165 Ma) in the Argo Abyssal Plain (Figure 1a), and rapidly propagated southwards during the Valanginian–Hauterivian (Figure 2; 140 Ma–130 Ma: Gaina, Mueller, Brown, Ishihara, & Ivanov, 2007; Markl, 1978; Mihut & Mueller, 1998; Veevers & Li, 1991), producing a rifted margin on the Australia–Antarctic plate, conjugate to Greater India. North of the Wallaby–Zenith Fracture Zone (Figure 1a), the rifted margin is voluminously magmatic, with extensive seaward-dipping reflector sequences (Direen et al., 2008; Planke, Symonds, Alvestad, & Skogseid, 2000), and high velocity lower crust, extending south into the Houtman Sub-basin (Figure 1a). In contrast, in the Zeewyck and Vlaming sub-basins of the Perth Basin (Figure 1a), no seaward-dipping reflector sequences or high velocity lower crust have been documented, and the margin is considered weakly magmatic (Bradshaw, Rollet, Totterdell, & Borissova, 2003), with the presence of discrete volcanic centres (Dadd, Kellerson, Borissova, & Nelson, 2015; Gorter & Deighton, 2002), which are also imaged seismically in the Mentelle Basin (Maloney et al., 2011). The volcanic margin north of the Wallaby–Zenith Fracture Zone predates the earliest currently known 124 Ma (Aptian) onset of Kerguelen Plateau-related hotspot volcanism (Duncan, 2002; Olierook et al., 2015).

The southern Australian continental margin east of the Naturaliste Plateau is not well studied (Bradshaw et al., 2003), but contains onshore volcanic and intrusive rocks of the Bunbury Basalt (Coffin & Eldholm, 1992; Duncan, 2002; Frey et al., 1996; Ingle, Scoates, Weis, Brugmann, & Kent, 2004; Olierook et al., 2016). The Bunbury Basalt contains two geochemical suites: the Casuarina and Gosselin suites (Frey et al., 1996), and three distinct phases of eruption, at  $136.96 \pm 0.43$  Ma,  $132.71 \pm 0.43$  Ma and  $130.45 \pm 0.82$  Ma (Olierook et al., 2016). The Bunbury Basalt has been correlated with the Rajmahal Traps (Figure 1a) of eastern India (Coffin & Eldholm, 1992; Frey et al., 1996; Kent et al., 1997), which are dated at  $118.1 \pm 0.3$  Ma (Kent et al., 2002). The Bunbury Basalt and Rajmahal Traps have been linked to the Kerguelen mantle hotspot

(Coffin & Eldholm, 1992; Duncan, 2002; Frey et al., 1996; Ingle et al., 2004; Kent et al., 1997; Olierook et al., 2016).

The southern margin of the Naturaliste Plateau, between Australia and Antarctica, began rifting in Jurassic time (Callovian: ca 165 Ma; Direen, 2011; Direen et al., 2007; Maloney et al., 2011; Tikku & Direen, 2008; Totterdell et al., 2000). At ca 95 Ma (Cenomanian) mafic volcanism occurred on the co-joined Broken Ridge and Kerguelen Plateau (Figures 1a and 2) (Duncan, 2002; Mutter & Cande, 1982; Tikku & Cande, 2000). Highly diachronous breakup between Australia and Antarctica and propagation of the Southeast Indian Ridge to the southeast in the late Cretaceous (Direen, Stagg, Symonds, & Norton, 2013; Tikku & Direen, 2008) formed a magma-poor, hyperextended margin (Direen et al., 2007, 2013; Direen, Stagg, Symonds, & Colwell, 2011; Sayers, Symonds, Direen, & Bernardel, 2001). Break-up south of the Naturaliste Plateau appears to have taken place between ca 90 and ca 84 Ma (Figure 2, Turonian–Santonian) (Beslier et al., 2004). Extreme thinning outpaced magma supply (e.g. Peron-Pinvidic & Manatschal, 2009), resulting in exhumation and marine flooding of the lower crust (Halpin et al., 2008) and mantle (Beslier et al., 2004) at the southern margin of the Naturaliste Plateau, and in the Diamantina Zone (Figure 1b), respectively.

**Existing geological knowledge and sampling of the Naturaliste Plateau**

Based on seismic and gravity data, the middle crust of the Naturaliste Plateau is incised by probable Paleozoic and Mesozoic rift basins (Borissova, 2002; Direen et al., 2007). The upper crust of the plateau comprises volcanic rocks and >2 km of post-Turonian sediments (Borissova, 2002; Burkle, Saito, & Ewing, 1967; Ford, 1975; Maloney et al., 2011).

The first basement samples from the Naturaliste Plateau were obtained by the USNS *Eltanin* in 1972, from a single site on the northeastern plateau (Figure 1b). This dredge recovered manganese crusts containing 0.5–15 cm conglomerate cobbles set in a matrix of manganese oxide and detrital grains of quartz, plagioclase, clinopyroxene, and garnet-bearing protoliths (Coleman, Michael, & Mutter, 1982; Heezen & Tharp, 1973). The cobbles were initially interpreted as continental fragments (Heezen & Tharp, 1973), but major and trace element analyses showed them to be mafic aphyric or plagioclase-phyric tholeiitic basalts (Coleman et al., 1982; Mahoney et al., 1995; Storey et al., 1992). The presence of cobbles indicates erosion and transport in a high-energy environment, of at least at or above wave base, implying the site of eruption of the lavas on the Naturaliste Plateau was not always as deeply submerged as it is today.

Further sampling of the Naturaliste Plateau was undertaken by the Deep Sea Drilling Project (DSDP). Two holes (Sites 258 and 264; Figure 1b) terminated in pre-Cenomanian and middle-late Albian sedimentary sequences (Davies et al., 1974; Ford, 1975; Hayes et al., 1975). Importantly, the lowermost 35 m at Site 264 recovered conglomerate containing abundant mafic clasts (Ford, 1975; Hayes et al., 1975). This shows that both the northeastern (Site 258) and southern (Site 264) plateau contain mafic lavas that could have been erupted at or above wave base.

In 1998, dredging from N/O *Marion Dufresne* recovered basalt lavas, dolerite, gabbro, and diorite, along with a small number of granite and gneiss fragments (Beslier et al., 2004).

## Sampling of the Naturaliste Plateau by the R/V *Southern Surveyor*

In 2005 the R/V *Southern Surveyor* dredged the steep margins of the plateau, with the best samples obtained from the southern flanks (Crawford, 2005; Figure 1b). Of 28 attempted bottom haul chain dredges, 11 yielded useable igneous rocks (Table 1; Figure 1b), 11 dredges were empty, and the remainder contained only sediments (Crawford, 2005). The igneous samples were dominantly mafic with varying degrees of seafloor alteration (Tables 1 and 2; Supplementary Papers Appendix 1). Some dredges recovered a mixture of rock types, including basalt lavas, dolerites, rhyolite, and granodiorite (Supplementary Papers Appendix 1), and were probably sampled from talus slopes comprising material from several lithostratigraphic units. Seafloor alteration was variable, ranging from minor to extreme, and usually takes the form of smectite replacing glass, and clay replacing plagioclase. The least altered samples from several dredges were selected for detailed petrographic and geochemical analysis.

The dredged basalt lavas are aphyric or plagioclase+augite-phyric and represent a variety of submarine eruption styles, including: massive lava, pillow lava lacking vesicles, lava breccia, hyaloclastite, and highly vesicular lava (Supplementary Papers Appendix 1). The sample suite does not contain material from unambiguously subaerial eruptions.

In addition to the lavas, some dredges recovered medium-grained rocks (e.g., dolerite, granophyre) presumably from intrusive units. Dolerite samples (DR7-2, 7-5, 10-39, 11-19, 11-25, 12-20, 13-7, 21-17) are uniformly medium-grained rocks composed of augite, plagioclase and Fe-Ti oxides. Felsic granophyre in DR10-16 (dredged with gabbro, DR10-14, dolerite DR10-39, and basalts DR10-7 10-67, 10-164) may derive from the last-crystallised part of a thick gabbroic or doleritic sill. Several blocks of formerly glassy, commonly spherulitic quartz+K-feldspar-phyric rhyolite (DR7-12, DR12-41) were recovered among the basalts and dolerites.

In addition to these mafic and felsic igneous rocks, two *Southern Surveyor* dredges (DR18 and DR21; Figure 1) also contained fragments of continental crustal rocks, comprising felsic gneiss, microcline phyric granite, felsic orthogneiss and hornblende-garnet gneissic diorite (Halpin et al., 2008). Within some thin metamorphic rims of Cambrian age (Halpin et al., 2008, and see below), zircon cores yielded U-Pb crystallisation ages of  $1177 \pm 28$  Ma (DR18-4, gneiss,  $n = 10$ ) and  $1154 \pm 25$  Ma (DR21-1, gneiss,  $n = 15$ ). Chemical (total U-Th-Pb) ages for monazites in two gneisses are much younger ( $515 \pm 5$  Ma DR18-4,  $n = 23$  analyses of 10 crystals;  $515 \pm 7$  Ma DR21-3,  $n = 49$  analyses of 23 crystals), and together with the zircon metamorphic rims, suggest that peak thermal metamorphism in these rocks was related to the Cambrian Pinjarra Orogeny of southwest Western Australia (Halpin et al., 2008). The presence of these old mid-crustal continental rocks at two *Southern Surveyor* and one *Marion Dufrense* dredge sites, along with the more widespread occurrence of mafic+felsic igneous activity, is consistent with seismic and gravity data that indicate that the plateau is underlain by thinned (12.5–16 km) continental crust capped by volcanic rocks (Direen et al., 2007), unlike initial suggestions that envisaged the plateau to be constructed entirely from juvenile oceanic erupted material (Coffin & Eldholm, 1992; Coleman et al., 1982).

## Geochronology

The age and duration of igneous activity on the southern Naturaliste Plateau was examined using  $^{40}\text{Ar}/^{39}\text{Ar}$  dating of plagioclase from a basalt and two dolerites and U-Pb dating of zircon from a granophyre, a monzodiorite and a rhyolite, all selected from the R/V *Southern Surveyor* dredge sample suites.



**Laser ablation ICP-MS zircon U–Pb dating**

LA-ICP-MS dating of zircons was carried out at the University of Tasmania (Supplementary Papers Appendix 3). Zircons were extracted from three of the more differentiated rocks, a granophyre (DR10-16), a monzodiorite (DR11-6), and a rhyolite (DR12-29). The zircons extracted from the three rocks are euhedral (some unbroken grains with both terminations; others are stubby) and are 50–120 µm in length. In cathodoluminescence images, all analysed grains show oscillatory or sector zoning (Supplementary Papers Figure A3-1). Some grains in monzodiorite DR11-6 show igneous resorption textures on their margins. There are no identifiable inherited cores or metamict textures. U contents vary widely (31–1923 ppm) and Th/U is typically >1 (0.98–10.10). The Pb–U isotopic results define indistinguishable lower intercept ages for the three populations: 131.8 ± 3.9 Ma (granophyre DR10-16), 128.2 ± 2.3 Ma (monzodiorite DR11-6) and 129.8 ± 6.1 Ma (rhyolite DR12-29, all ages ± 2σ; Figure 3).

**<sup>40</sup>Ar/<sup>39</sup>Ar dating of basaltic plagioclase**

Three basaltic samples with well-preserved plagioclase were selected for <sup>40</sup>Ar/<sup>39</sup>Ar dating. Basalt DR11-19 contains plagioclase phenocrysts ≤5 mm long in a grey groundmass; dolerite DR12-8 has plagioclase <1 mm long set in a mid-brown groundmass; and dolerite DR13-33 has plagioclase phenocrysts ≤15 mm long set in a light-brown groundmass. A description of the analytical methods and results is presented in Supplementary Papers Appendix 4.

Plagioclases from DR11-19 and DR12-8 yield precise plateau ages of 129.4 ± 1.3 and 130.6 ± 1.2 Ma (2σ), respectively, reflecting their relatively high K/Ca ratios and radiogenic <sup>40</sup>Ar yields (Figure 4). DR13-33 yields a plateau age of 130 ± 4 Ma (2 σ), with the inferior age precision reflecting smaller sample size, lower K/Ca and lower radiogenic <sup>40</sup>Ar yields. The step-heating sequences for both DR11-19 and DR12-8 show declining %<sup>40</sup>Ar\* values at high temperature, reflecting increased atmospheric argon contributions from the resistance furnace itself; however, this has no influence on the derived <sup>40</sup>Ar/<sup>39</sup>Ar ages.

Initial <sup>40</sup>Ar/<sup>36</sup>Ar ratios on isochron diagrams (Figure 4) are within error of modern-day atmospheric Ar, indicating the analysed plagioclase samples are free from inherited argon. While the low-temperature steps yield younger ages – attributed here to argon loss caused by incipient seawater alteration of the plagioclase – the reported plateau <sup>40</sup>Ar/<sup>39</sup>Ar ages are based on 64 to 82% of the <sup>39</sup>Ar released, indicating they are reliable determinations of plagioclase crystallisation ages. This is supported by concordant <sup>40</sup>Ar/<sup>39</sup>Ar isochron and plateau ages.

The U–Pb zircon and <sup>40</sup>Ar/<sup>39</sup>Ar plagioclase ages overlap within their reported uncertainties and range from 131.8 ± 3.9 to 128.2 ± 2.3 Ma, placing volcanic activity in this sector of the plateau in the late Hauterivian to Barremian, possibly just post-dating the ca 132 Ma Valanginian–Hauterivian regional unconformity (Maloney et al., 2011).

**Geochemistry**

Concentrations of major and trace elements in 47 samples of basalts, dolerites, rhyolite and granophyre were determined by X-Ray fluorescence (XRF) and solution-mode ICP-MS (University of Tasmania), and are reported in Tables 2 to 4. Sr–Nd–Pb–Hf isotopic compositions were measured by multi-collector ICP-MS (University of Melbourne) and are reported in Table 5. Details of the analytical methods can be found in the Supplementary Papers (Appendices 2 and 5).

## Major elements

The dredge samples from the Southern Surveyor 2005 cruise analysed here vary widely in composition (48.0–75.5 wt% SiO<sub>2</sub>, 0.16 to 7.3 wt% MgO; Table 2). Loss on Ignition (LOI) ranges from 0.82 to 7.25 wt%, with only 6 of the 46 analysed samples having <2 wt% LOI (Table 2). LOI is a broad measure of low-temperature alteration, and these results illustrate the extent of seawater alteration in the samples. Ca, Na and K are particularly mobile during submarine alteration (e.g. Hart, Erlank, & Kable, 1974) and their concentrations in the dredge samples are thus unlikely to be primary.

All mafic samples have <8 wt% MgO (most have 5–7 wt% MgO and 48–53 wt% SiO<sub>2</sub>; Figure 5a) indicating they represent relatively evolved magmas. The most differentiated members of this group have 2–4% MgO and up to 56 wt% SiO<sub>2</sub>. Al<sub>2</sub>O<sub>3</sub> is high compared with many other basaltic suites (13 samples with >18 wt%, see Table 2), and CaO/Al<sub>2</sub>O<sub>3</sub> is low (<0.6) in most analysed samples. This may reflect accumulation of Al-rich plagioclase (Bryan, Thompson, & Ludden, 1981), consistent with prominent plagioclase phenocrysts in the lavas. Although there is much scatter (perhaps partly related to Ca mobility), CaO/Al<sub>2</sub>O<sub>3</sub> tends to be lower at low MgO and approaches zero in the most silicic samples (DR10-16 and 12-41) and in DSDP Site 264 core material. In addition to plagioclase, a Ca-rich mineral – probably clinopyroxene – must have been an important fractionating phase. TiO<sub>2</sub> (0.79–3.41 wt% in basaltic samples) shows a broad anti-correlation with MgO (Figure 5b). Low TiO<sub>2</sub> (<0.3 wt%) in the four SiO<sub>2</sub>-rich lavas indicates fractionation of a Fe–Ti oxide; the high magnetic susceptibilities recorded for the mafic samples suggest this is probably Ti-magnetite.

The most silicic samples analysed here have ~75 wt% SiO<sub>2</sub>, low Fe, Mg and Ca, and high Na and K (Table 2; Figure 5a, c). Silicic samples were also recovered at DSDP Site 264 (Coleman et al., 1982).

## Trace elements

Trace element concentrations (Tables 3 and 4) show variations typical of basaltic systems: most incompatible elements (Zr, Nb, Hf, Ta, REE, Y, Th, U, Rb, Ba, Pb) are anti-correlated with Mg while Cr, Ni, Cu and Co show positive correlations. Many trends are scattered, undoubtedly reflecting alteration effects (Figure 6a). Co-variations among alteration-resistant elements (e.g. Nb, Zr, LREE) show much less scatter (Figure 6b, c). However, given the large geographic spread of the dredge samples, primary variations of trace element abundances, as well as local differentiation effects, probably contribute to the observed scatter.

The composition of mafic rocks varies with tectonic setting and the degree of partial melting; high degrees of partial melting typically produce tholeiitic magmas, which are relatively depleted in incompatible elements, while low degrees of melting typically produce alkaline magmas, which are enriched in incompatible elements. To determine the relative extent of melting, it is important to determine if the Naturaliste Plateau dredge samples are tholeiitic or alkaline. Classification using the total alkalis (Na<sub>2</sub>O+K<sub>2</sub>O) versus SiO<sub>2</sub> diagram (TAS; Le Bas, Le Maitre, Streckeisen, & Zanettin, 1986) is compromised by seawater alteration, and the results of a TAS classification (18 of the 45 dredge samples plot in the alkaline field; Figure 5c) are likely to be spurious. An alternative subalkaline vs alkaline classification can be made using the alteration-resistant high field strength elements (Pearce & Cann, 1973), such as the Nb/Y ratio (Pearce & Norry, 1979), which identifies the Naturaliste Plateau samples as dominantly tholeiitic (Figure 5d).

Rare-earth element (REE) concentrations for 15 samples from eight of the nine sampled dredges are anti-correlated with MgO and have unfractionated to LREE-enriched normalised distribution patterns (Figure 7a), with La/Lu<sub>PM</sub> ranging from 1.28 to 7.24 in the basalts and from 4.5 to 11.3 in two silicic rocks (Table 4, subscript 'PM' denotes primitive mantle-normalised values, relative to values in McDonough & Sun, 1995). HREE fractionation is modest (Gd/Lu<sub>PM</sub> 1.0–2.4). Some of the basaltic samples have patterns resembling those typical of Indian Ocean MORB while others match the patterns in Kerguelen Plateau basalts from ODP Site 1138 that have been proposed as melts derived from the hotspot at ca 100 Ma (Neal, Mahoney, & Chazey, 2002).

Eu/Eu\* (0.79–1.21 in the basalts, 0.36–0.54 in the silicic rocks) varies considerably and is undoubtedly controlled by plagioclase fractionation (viz. petrographic evidence and correlation with Al<sub>2</sub>O<sub>3</sub>). However, correlation with other parameters (e.g. La/Sm, Zr and radiogenic isotopes) suggest further controls, such as addition of a crustal component in some samples.

**Sr–Nd–Pb–Hf isotopes**

The radiogenic isotope compositions (Table 5) for nine of the least altered samples representing seven of nine dredges are highly heterogeneous. For example, parent/daughter ratios in eight basalts vary widely (<sup>87</sup>Rb/<sup>86</sup>Sr 0.03–1.13, <sup>147</sup>Sm/<sup>144</sup>Nd 0.139–0.203, <sup>176</sup>Lu/<sup>177</sup>Hf 0.012–0.028, <sup>238</sup>U/<sup>204</sup>Pb 2.2–20.9, <sup>232</sup>Th/<sup>204</sup>Pb 9.4–54.9; Table 5). The respective values in rhyolite 12-41 are 3.65, 0.111, 0.0120, 4.6 and 79.9. The measured isotopic ranges for the basalts are: <sup>87</sup>Sr/<sup>86</sup>Sr 0.7038 to 0.7147, ε<sub>Nd</sub> +4.4 to –10.6, ε<sub>Hf</sub> +4.7 to –15.7, <sup>206</sup>Pb/<sup>204</sup>Pb 17.28 to 18.32 and <sup>208</sup>Pb/<sup>204</sup>Pb 38.15 to 39.24 (Table 5). After age correction to 130 Ma, the average of the U–Pb zircon and plagioclase <sup>40</sup>Ar/<sup>39</sup>Ar ages obtained here, <sup>87</sup>Sr/<sup>86</sup>Sr<sub>i</sub>, <sup>143</sup>Nd/<sup>144</sup>Nd<sub>i</sub> and <sup>176</sup>Hf/<sup>177</sup>Hf<sub>i</sub> in the mafic rocks range from 0.7036 to 0.7135, 0.51268 to 0.51197 (ε<sub>Nd</sub> +4.3 to –9.7) and 0.28291 to 0.28231 (ε<sub>Hf</sub> +7.2 to –14.1), respectively (Table 5). These isotopic compositions show consistent correlations with each other and with chemical indices of differentiation, e.g. Si, Mg, Ti, and Zr concentrations (Figures 5 and 6). While we will argue below that this reflects crustal contamination, it also indicates that calculated <sup>87</sup>Sr/<sup>86</sup>Sr<sub>i</sub> ratios in the acid-leached samples are good estimates of primary <sup>87</sup>Sr/<sup>86</sup>Sr, despite the alteration experienced by the samples. Initial isotope ratios in rhyolite DR12-41 (<sup>87</sup>Sr/<sup>86</sup>Sr<sub>i</sub> 0.7175, ε<sub>Nd</sub> –15.8, ε<sub>Hf</sub> –18.8) extend the trends on Sr–Nd–Hf isotope plots and in plots of Sr–Nd–Hf isotopes versus Si, Mg and Zr, but not Ti, probably because Ti is strongly fractionated in the parental magmas of the most felsic rocks (Figure 5).

Initial Pb isotope ratios (<sup>206</sup>Pb/<sup>204</sup>Pb 17.23–18.26, <sup>207</sup>Pb/<sup>204</sup>Pb 15.58–15.68, <sup>208</sup>Pb/<sup>204</sup>Pb 37.94–38.92; Table 5; Figure 8) do not show strong correlations with each other, with Sr–Nd–Hf isotopes, or with chemical parameters, despite the relatively modest age corrections (<sup>206</sup>Pb/<sup>204</sup>Pb ≤0.12 and <sup>208</sup>Pb/<sup>204</sup>Pb <0.30 in eight of nine samples). This lack of correlation suggests that either alteration effects are not sufficiently removed by the strong acid leaching of the analysed rock chips, and/or that primary Pb isotope variations were heterogeneous.

The large ranges in Sr–Nd–Hf isotopic ratios and their correlations with chemical compositions (Figures 5, 6 and 8), as well as trace element evidence (high ratios of Th/Nb and La/Nb in the mafic rocks; Figure 7), and the geological setting of the ca 130 Ma volcanic rocks on attenuated older continental crust, strongly indicate these results reflect a crustal contamination trend. This trend, defined by the mafic rocks, appears to be controlled by the same crustal component that is even more strongly expressed in the coeval rhyolite, DR12-41. Simple binary mixing lines between model mantle- and crustally-derived end-members (Figure 8, details for end-members

in figure caption) encompass, or pass close to, the data for the southern Naturaliste Plateau, and all other data sets plotted in these figures. The crustal end-member is based on published data for the Albany Fraser Orogen in southern Western Australia (Fletcher et al., 1983; Kirkland et al., 2011; Rosman, Wilde, Libby, & De Laeter, 1980), which was considered the most likely onshore equivalent of granites and granitic gneisses recovered from the same *Southern Surveyor* dredges that yielded the basaltic material discussed here (Halpin et al., 2008).  $\epsilon_{\text{Nd}}$  in the crustal end-member is based on the average of a large Nd isotope data set for the Albany Fraser Orogen (H. Smithies, pers. comm., augmented by data from Fletcher et al., 1983,  $\epsilon_{\text{Nd130}} -19 \pm 5, \pm 1 \sigma, n = 70$ ).  $\epsilon_{\text{Hf}}$  is based on zircon-Hf isotope data reported in Kirkland et al. (2011). For our purpose, the initial  $^{176}\text{Hf}/^{177}\text{Hf}$  recorded in the dated magmatic zircons (ca 1.35, 1.65–1.75 Ga) were ‘aged’ to 130 Ma using an average crustal  $^{176}\text{Lu}/^{177}\text{Hf}$  of 0.015 (Goodge & Vervoort, 2006), to yield a range of  $\epsilon_{\text{Hf130}}$  of  $-17$  to  $-26$ .  $^{87}\text{Sr}/^{86}\text{Sr}$  in the Albany Fraser Orogen is more difficult to estimate because strong heterogeneity is likely and because there are few published data.  $^{87}\text{Sr}/^{86}\text{Sr}_{130}$  ratios for Meso- to Neoproterozoic granites and sedimentary rocks in the western part of the orogen (Rosman et al., 1980; Turek & Stephenson, 1966) are very high ( $>0.740$ ), consistent with simple modelling of Rb-rich rocks of this age; we chose a  $^{87}\text{Sr}/^{86}\text{Sr}_{130}$  of 0.74 for the model crustal end-member.

While the particular end-member compositions used here may not be representative or unique, they are plausible within the regional geological context and fit the data reasonably well. Based on the models, up to 70–75% of the Hf and Nd in rhyolite DR12-41 could be crustally derived. The least-contaminated samples, with positive  $\epsilon_{\text{Nd}} - \epsilon_{\text{Hf}}$  and  $^{87}\text{Sr}/^{86}\text{Sr}$  of 0.7036–0.7046, contain  $<10\%$  of the model crustal end-member. We note that data for basalts from the northern Naturaliste Plateau, from the onshore Bunbury and Rajmahal basalts, and for Cretaceous basalts from the Kerguelen Plateau and Broken Ridge are equally well described by these simple mixing curves, despite their very different geological locations.

The Sr–Nd isotope data for basalts dredged from the northern Naturaliste Plateau (Eltanin Cruise, ‘NNP’ in Figure 8) resemble those for the southern margin rocks (Figure 8) but Pb isotope data follow different trends, with some samples close to the field for modern MORB from the Southeast Indian Ridge (Figure 8c, d).

## Discussion

### Comparison of Naturaliste Plateau basalt with the Bunbury Basalt in southwest Australia

The compositions of mafic rocks from the Naturaliste Plateau and those from the near-coeval on-shore Bunbury Basalt overlap substantially, despite the much more limited compositional range of the on-shore basalts (Figures 5–7). Both suites show variable upper crustal signatures, e.g. in the Th/Nb vs. La/Nb plot (Figure 7) where all samples lie on a trend from primitive mantle towards the composition of average upper continental crust, with Naturalist Plateau rhyolite DR12-41 showing the highest Th/Nb and La/Nb ratios. Mafic rocks dredged by USNS *Eltanin* from Site 55-12 on the northwest margin of the Naturaliste Plateau (Coleman et al., 1982) (Figure 1) are similarly evolved, and those basalts less enriched in cumulus plagioclase phenocrysts show also high  $\text{SiO}_2$  (mainly 54–57 wt%), like the more fractionated among our dredged Naturaliste Plateau basalts. Mahoney et al. (1995) found that the *Eltanin* basalts have flat to slightly LREE-enriched REE patterns, like those from the southern margin of the Naturaliste Plateau, and they show similar large ranges in Th/Nb and La/Nb (Figure 7).

The overlap in age (137–130 Ma vs ca 130 Ma) and composition strongly imply a spatial continuity between the Bunbury Basalts and basaltic rocks from the southern margin of the Naturaliste Plateau. Although undated, available geochemical data suggest that it is also likely that the mafic samples dredged from USNS *Eltanin* on the northwest margin of the Naturaliste Plateau are part of the same magmatic province, as suggested by Mahoney et al. (1995).

**Comparison between the Naturaliste and Kerguelen plateaus**

Cretaceous basaltic rocks from the Naturaliste Plateau (and from the onshore Bunbury Basalt) generally have higher SiO<sub>2</sub> contents (50–60 wt%) than basalts from the Kerguelen Plateau (e.g. ODP Site 1138, 45–50 wt%; Figure 5). However, evolved compositions like those from the Naturaliste Plateau also occur on the Kerguelen Plateau, e.g. dacite forms the uppermost flow drilled at ODP Site 1138 (Neal et al., 2002). Apparently as construction of the two igneous plateaus terminated, the flux of mantle-derived basaltic magma slowed sufficiently to enable formation of SiO<sub>2</sub>-rich magma. Plagioclase-rich rocks like those found on the Naturaliste Plateau are also dominant at ODP Site 757 on the Ninetyeast Ridge (Frey, Jones, Davies, & Weis, 1991). TiO<sub>2</sub> concentrations in Naturaliste Plateau basaltic rocks scatter strongly, reaching both lower and higher levels than those recorded at ODP Sites 1138 and 738 (Figure 5).

Isotopic (Sr–Nd–Pb–Hf) data for several tholeiitic mafic suites from the Kerguelen Plateau show trends towards evolved signatures similar to old continental crust. These include sites on the southern Kerguelen Plateau (ODP Site 738), from Elan Bank (ODP Site 1137) and from its conjugate margin, Broken Ridge (R/V *Conrad* dredge 8; Coffin et al., 2002; Davies et al., 1989; Frey, Weis, Borisova, & Xu, 2002; Ingle, Weis, & Frey, 2002a; Ingle, Weis, Scoates, & Frey, 2002b; Ingle et al., 2004; Mahoney et al., 1995; Storey et al., 1992). Mahoney et al. (1995) argued that these isotopic signatures signal ‘shallow-level incorporation of continental lithosphere in either the head of the early Kerguelen plume or in plume-derived magmas’ at ‘sites located closest to rifted continental margins’. The strong continental lithospheric signature observed in the Cretaceous dredge samples from the southern Naturaliste Plateau, like that observed in the Bunbury Basalt (Frey et al., 1996), supports this argument. Furthermore, the correlations of some major and trace elements with isotopic compositions (Figures 5 and 6) in the southern Naturaliste Plateau samples strongly indicate that the continental signature in these rocks was acquired at crustal level. The large geographic spread of the dredge samples and their strongly variable chemical and isotopic compositions (even within the same dredge, see data for DR7 and DR12; Table 5) imply they represent broadly coeval but spatially separate volcanic centres, each with its own magmatic history but involving the same (or similar) juvenile and crustal components (Figure 8). The presence of exhumed lower continental crystalline Mesoproterozoic crust beneath the volcanic carapace of the Naturaliste Plateau (Halpin et al., 2008) and other sectors of offshore Western Australia (Williams, Whittaker, Granot, & Mueller, 2013), provides a suitable setting and obvious source for the inferred crustal component in the Cretaceous basalts. This is illustrated in Figure 9, which shows the isotope data of Figure 8 with some inferred source components (see also Ingle, Weis, Doucet, & Mattielli, 2003). In Hf–Pb isotope space (Figure 9a), for example, the southern Naturaliste Plateau basalts appear to be dispersed between the putative Kerguelen plume head component and a lower crustal component. Local granite gneisses from the same *Southern Surveyor* dredges have suitable compositions to represent this crustal source. The radiogenic Pb data (Figure 9b) are more difficult to interpret in terms of the mantle source (or sources involved) but a Lower Crust component (generally thought to be associated with low <sup>206</sup>Pb/<sup>204</sup>Pb, see Ingle et al., 2002) is again implied by the data trend. The *Southern Surveyor* gneiss samples shown in Figure 9a are not a suitable match to the

crustal component in the southern Naturaliste Plateau (SNP) basalts, as their  $^{208}\text{Pb}/^{204}\text{Pb}$  is far too high. The crustal basement of the Naturaliste Plateau thus is likely to be very heterogeneous, in particular in its Sr–Pb isotope composition.

### A rift-fragmented Large Igneous Province in the eastern Indian Ocean

Extensive dredging and geochronology from R/V *Southern Surveyor* cruise SS09/2005, together with seismic reflection data (Borissova, 2002; Maloney et al., 2011), potential field analyses (Direen et al., 2007), and DSDP data (Burkle et al., 1967; Ford, 1975) indicate that an extensive post-Valanginian volcanic carapace erupted over the Naturaliste Plateau and the adjacent Mentelle Basin (Maloney et al., 2011). This volcanic carapace formed a major unconformable landscape surface correlative with a similar surface in the Perth Basin, where it has also been drilled and dated (Bradshaw et al., 2003; Dadd et al., 2015; Gorter & Deighton, 2002). Above this surface are developed major, kilometre thick, seismically reflective, high velocity mounded edifices (Maloney et al., 2011), likely to be mafic volcanoes (Gorter & Deighton, 2002).

The discovery of major Cretaceous basaltic volcanism mantling the Naturaliste Plateau (this study) greatly expands the known volume of ca 130 Ma basaltic volcanism in the eastern and northern margins of the wider Indian Ocean basin (Coffin et al., 2002; Duncan, 2002; Frey et al., 1996; Ingle et al., 2004; Olierook et al., 2016; Zhu et al., 2008). The area of the Naturaliste Plateau over which this Early Cretaceous volcanic surface has been encountered is  $\sim 90\,000\text{ km}^2$  (this study; Figure 1). Additional extensive early Cretaceous basaltic volcanism within the Australian region (Figure 1) that can be correlated to the Naturaliste Plateau in both age and composition occurs in the Mentelle Basin (see above,  $\sim 44\,000\text{ km}^2$ ; Maloney et al., 2011) and the ca 124 Ma Wallaby Plateau ( $\sim 70\,000\text{ km}^2$ , Olierook et al., 2015); the onshore 137–130 Ma Bunbury Basalts of the Perth Basin (Olierook et al., 2016) cover a relatively small area. Elsewhere, additional correlatives include  $\sim 40\,000\text{ km}^2$  of the Comei-Cona basalt suites in Tibet (Zhu et al., 2008, 2009), the Valanginian volcanic sectors of the Enderby Basin (Stagg et al., 2004), and the Princess Elizabeth Trough (Stagg, Colwell, Borissova, Ishihara, & Bernardel, 2006) on the Antarctic Plate. Together, these geochemically similar 136–124 Ma basaltic volcanics cover a minimum total area of  $\sim 244\,000\text{ km}^2$ . Assuming a thickness of 0.5–1 km (Direen et al., 2007; Frey et al., 1996; Maloney et al., 2011; Zhu et al., 2008, 2009), the minimum erupted volume is  $\sim 1.2 \times 10^6\text{ km}^3$ , establishing the 137–124 Ma Naturaliste–Bunbury–Wallaby–Comei–Cona–Enderby–Antarctic province as a LIP in its own right (Coffin & Eldholm, 1992).

Geochemical and isotopic data (e.g. Davies et al., 1989; Duncan, 2002; Frey et al., 1996, 2002; Ingle et al., 2002a, 2002b, 2003, 2004; Kent et al., 1997, 2002; Mahoney et al., 1995; Neal et al., 2002; Storey et al., 1992; Zhu et al., 2008, 2009; this study) indicate similarities between these ca 130 Ma magmatic rocks and the oldest eruptive phases in the Kerguelen Plateau (ODP Site 1138: Coffin et al., 2002). Perhaps the most noticeable shared feature is the occurrence of Nb-depleted basalts (Figure 7d). A characteristic of the continental crust, Nb depletions are observed in Cretaceous basalts from ODP sites 738 and 1137 on the Kerguelen Plateau, in the Rajmahal Traps, Bunbury Basalt, Wallaby Basin and on the Naturaliste Plateau.

### Conclusions

Similarities in age, major and trace element composition, and Sr–Nd–Hf–Pb isotopic ratios in the now widely dispersed fragments of early Kerguelen hotspot magmatism, including rocks in southeast Tibet (Zhu et al., 2008, 2009), northeast India (Kent et al., 1997, 2002), southwest Western Australia (Frey et al., 1996; Ingle et al., 2004; Olierook et al., 2016), Wallaby Plateau

(Olierook et al., 2015) and the Naturaliste Plateau (this study) document LIP formation at 137–124 Ma. This LIP predates the earliest known stages recorded from the Kerguelen Plateau (ca 120 Ma: Coffin et al., 2002, Duncan, 2002) although we note that the currently deepest penetration of Kerguelen Plateau igneous basement is only 233 m of an estimated ~20 km total thickness (Coffin et al., 2000); older Cretaceous eruptions may yet be found on the Kerguelen Plateau. The extensive layer-cake stratigraphy of the 0.5–1 km-thick seismically defined mafic cover of the Naturaliste Plateau (Borissova, 2002; Direen et al., 2007), and the absence of seaward-dipping reflector sequence crustal architecture that dominates the Australian margin north of the Wallaby–Zenith Fracture Zone (Direen et al., 2008; Planke et al., 2000), indicates that this plateau and the adjacent Mentelle Basin represent a ~130 000 km<sup>2</sup> fragment of the Kerguelen LIP, rather than breakup-related volcanism at the margin of continental plates.

If the extensive basaltic volcanism on the Naturaliste Plateau and Mentelle Basin is indeed an early stage of the Kerguelen hotspot volcanism, models involving an “incubating plume” (Coffin et al., 2002; Ingle et al., 2002, 2004; Kent et al., 1992; Zhu et al., 2008, 2009) are no longer necessary to explain the apparent age difference between this magmatic activity and the oldest known volcanism on the Kerguelen Plateau. It also confirms that the Kerguelen hotspot did not trigger the contemporaneous continental breakup, even if correlation with the Naturaliste–Bunbury sequences now mean that its earliest recorded products could be as old as 137 Ma, because breakup was already underway and progressing from north (Direen et al., 2008; Mihut & Mueller, 1998) to south (Bradshaw et al., 2003; Markl, 1978; Powell et al., 1988) to southwest (Gaina et al., 2007; Stagg et al., 2004). The role of mantle plumes or hotspots as a trigger for breakup was also recently questioned for the South Atlantic Ocean (Fromm et al., 2015). Open questions remain about the possible role of large plate-boundary-forming stresses related to rifting in the post-breakup formation of this LIP.

**Acknowledgements**

We thank Master Ian Taylor, the ship’s crew, and the technical and scientific staff of R/V *Southern Surveyor* Voyage SS09/2005. AJC acknowledges Australian Research Council (ARC) grant DP0666062, and financial support of the Major National Research Facility for the R/V *Southern Surveyor* cruise SS09/2005, as well as analytical support from Geoscience Australia. NGD acknowledges the support of FROGTECH Pty Ltd in pursuing this research during the period 2006–2013. The <sup>40</sup>Ar/<sup>39</sup>Ar analyses were carried out at, and partially funded by, the UQ-AGES laboratory at The University of Queensland, and we gratefully acknowledge the support provided by P. Vasconcelos and D. Thiede. JMW acknowledges ARC grant DE150130. We thank K. Dadd and J. Foden for their reviews, and G. Caprarelli for editorial handling. An earlier version of this manuscript was improved by reviews from A. Kerr and an anonymous reviewer.

**Supplementary papers**

- Appendix 1. Photographs of dredge samples, RV Southern Explorer voyage 2005.
- Appendix 2. Major and trace element analysis (University of Tasmania).
- Appendix 3. Laser-ablation ICP-MS U–Pb zircon dating (University of Tasmania).
- Appendix 4. <sup>40</sup>Ar/<sup>39</sup>Ar dating of plagioclase (University of Queensland).

Appendix 5. Radiogenic (Sr–Nd–Hf–Pb) isotopes (University of Melbourne).

## References

- Beslier, M. O., Royer, J. Y., Girardeau, J., Hill, P. J., Boeuf, E., Buchanan, C., Chatin, F., Jacovetti, G., Moreau, A., Munsch, M., Partouche, C., Robert, U., & Thomas, S. (2004). Une large transition continent–ocean en pied de marge sud-ouest australienne: premiers resultats de la campagne MARGAU/MD110. *Bulletin Societe geologique Francaise*, 175, 629–641.
- Borissova, I. (2002). *Geological framework of the Naturaliste Plateau*. Canberra ACT: Geoscience Australia Record 2002/20.
- Bradshaw, B. E., Rollet, N., Totterdell, J. M., & Borissova, I. (2003). *A revised structural framework for frontier basins on the southern and southwestern Australian continental margin*. Canberra ACT: Geoscience Australia Record 2003/03.
- Bryan, W. B., Thompson, G., & Ludden, J. N. (1981). Compositional variation in normal MORB from 22°–25°N: Mid-Atlantic Ridge and Kane Fracture Zone. *Journal of Geophysical Research: Solid Earth*, 86, 11 815–11 836.
- Burkle, L. H., Saito, T., & Ewing, M. (1967). A Cretaceous (Turonian) core from the Naturaliste Plateau. *Deep-sea Research*, 14, 421–426.
- Coffin, M. F., & Eldholm, O. (1992). Volcanism and continental break-up; a global compilation of large igneous provinces. In B. C. Storey, T. Alabaster & R. J. Pankhurst (Eds.), *Magmatism and the causes of continental break-up* (pp. 17–30). London, UK: Geological Society (London) Special Publications.
- Coffin, M. F., Frey, F. A., Wallace, P. J., et al. (2000). Proceedings of the Ocean Drilling Program, Initial Reports, 183 [Online]. Available from: [http://www-odp.tamu.edu/publications/183\\_IR/183ir.htm](http://www-odp.tamu.edu/publications/183_IR/183ir.htm).
- Coffin, M. F., Pringle, M. S., Duncan, R. A., Gladchenko, T. P., Storey, M., Müller, R. D., & Gahagan, L. A. (2002). Kerguelen hotspot magma output since 130 Ma. *Journal of Petrology*, 43, 1121–1139.
- Coleman, P. J., Michael, P. J., & Mutter, J. C. (1982). The origin of the Naturaliste Plateau, SE Indian Ocean; implications from dredged basalts. *Journal of the Geological Society of Australia*, 29, 457–468.
- Crawford, A. J. (2005). *Voyage Summary SS09/2005*. Hobart Tas: CSIRO, 10 pp.
- Dadd, K. A., Kellerson, L., Borissova, I., & Nelson, G. (2015). Multiple sources for volcanic rocks dredged from the Western Australian rifted margin. *Marine Geology*, 368, 42–57.
- Davies, H. L., Sun, S.-S., Frey, F. A., Gautier, I., McCulloch, M. T., Price, R. C., Bassias, Y., Klootwijk, C., & Leclaire, L. (1989). Basalt basement from the Kerguelen Plateau and the trail of a Dupal plume. *Contributions to Mineralogy and Petrology*, 103, 457–469.
- Davies, T. A., Luyendyk, B. P., Rodolfo, K. S., Kempe, D. R. C., McKelvey, B. C., Leidy, R. D., Horvath, G. J., Hyndmann, R. D., Thierstein, H. R., Herb, R. C., Boltovskoy, E., & Doyle, P. (1974). *Site*



258, *Initial Reports of the Deep Sea Drilling Program* (pp. 359–414). Washington DC: U.S. Government Printing Office.

Direen, N. G. (2011). Comment on “Antarctica — Before and after Gondwana” by S. D. Boger, *Gondwana Research*, 19, 335–371. *Gondwana Research*, 21, 302–304.

Direen, N. G., Borissova, I., Stagg, H. M. J., Colwell, J. B., & Symonds, P. A. (2007). Nature of the continent–ocean transition zone along the southern Australian continental margin: a comparison of the Naturaliste Plateau, SW Australia, and the central Great Australian Bight sectors. In G. D. Karner, G. Manatschal & L. M. Pinheiro (Eds.), *Imaging, Mapping and Modelling Continental Lithosphere Extension and Breakup* (pp. 235–261). London UK: Geological Society (London) Special Publications 282.

Direen, N. G., Stagg, H. M. J., Symonds, P. A., & Colwell, J. B. (2008). Architecture of volcanic rifted margins: new insights from the Exmouth–Gascoyne margin, Western Australia. *Australian Journal of Earth Sciences*, 55, 341–363.

Direen, N. G., Stagg, H. M. J., Symonds, P. A., & Colwell, J. B. (2011). Dominant symmetry of a conjugate southern Australian and East Antarctic magma-poor rifted margin segment. *Geochemistry Geophysics Geosystems*, 12, 10.1029/2010gc003306.

Direen, N. G., Stagg, H. M. J., Symonds, P. A., & Norton, I. O. (2013). Variations in rift symmetry: cautionary examples from the Southern Rift System (Australia–Antarctica), In W. U. Mohriak, A. Danforth, P. J. Post, D. E. Brown, G. C. Tari, M. Nemčok & S. T. Sinha (Eds.), *Conjugate Divergent Margins* (pp. 453–475). London UK: Geological Society (London) Special Publication 369.

Duncan, R. A. (2002). A time frame for construction of the Kerguelen Plateau and Broken Ridge. *Journal of Petrology*, 43, 1109–1119.

Fitton, J. G., Larsen, L. M., Saunders, A. D., Hardarson, B. S., & Kempton, P. D. (2000). Palaeogene continental to oceanic magmatism on the SE Greenland continental margin at 63°N: a review of the results of Ocean Drilling Program Legs 152 and 163. *Journal of Petrology*, 41, 951–966.

Fletcher, I., Wilde, S., Libby, W., Rosman, K., 1983. Sm-Nd model ages across the margins of the Archaean Yilgarn Block, Western Australia—II; southwest transect into the Proterozoic Albany-Fraser Province. *Journal of the Geological Society of Australia*, 30, 333–340.

Ford, A. B. (1975). Volcanic rocks of Naturaliste Plateau, Eastern Indian Ocean, Site 264, DSDP Leg 28. In D. E. Hayes, L. A. Frakes, P. J. Barrett, D. A. Burns, P.-H. Chen, A. B. Ford, A. G. Kaneps, E. M. Kemp, D. W. McCollum, D. J. W. Piper, R. E. Wall & P. N. Webb (Eds.), *Initial Reports of the Deep Sea Drilling Project* (pp. 821–833). Washington DC: U.S. Government Printing Office.

Frey, F., Jones, W., Davies, H., & Weis, D. (1991). Geochemical and petrologic data for basalts from Sites 756, 757, and 758: implications for the origin and evolution of Ninetyeast Ridge. *Proceedings of the Ocean Drilling Program Scientific Results* (pp. 611–659). Washington DC: U.S. Government Printing Office.

- 1  
2  
3 Frey, F. A., McNaughton, N. J., Nelson, D. R., de Laeter, J. R., & Duncan, R. A. (1996). Petrogenesis  
4 of the Bunbury Basalt, Western Australia: interaction between the Kerguelen plume and  
5 Gondwana lithosphere? *Earth and Planetary Science Letters*, 144, 163–183.  
6
- 7 Frey, F. A., Weis, D., Borisova, A. Y., & Xu, G. (2002). Involvement of continental crust in the  
8 formation of the Cretaceous Kerguelen Plateau: New perspectives from ODP Leg 120 sites.  
9 *Journal of Petrology*, 43, 1207–1239.  
10
- 11 Fromm, T., Planert, L., Jokat, W., Ryberg, T., Behrmann, J. H., Weber, M., & Haberland, C. (2015).  
12 South Atlantic opening: A plume-induced breakup? *Geology*, 43, 931–934.  
13
- 14 Gaina, C., Mueller, R. D., Brown, B., Ishihara, T., & Ivanov, S. (2007). Breakup and early seafloor  
15 spreading between India and Antarctica. *Geophysical Journal International*, 170, 151–169.  
16
- 17 Goodge, J. W., & Vervoort, J. D. (2006). Origin of Mesoproterozoic A-type granites in Laurentia: Hf  
18 isotope evidence. *Earth and Planetary Science Letters*, 243, 711–731.  
19
- 20 Gorter, J. D., & Deighton, I. (2002). Effects of igneous activity in the offshore northern Perth  
21 Basin; evidence from petroleum exploration wells, 2D seismic and magnetic surveys. In M.  
22 Keep & S. J. Moss (Eds.), *The Sedimentary Basins of Western Australia 3; Proceedings of the*  
23 *West Australian Basins Symposium*. Perth, WA: Petroleum Exploration Society of Australia.  
24
- 25 Graham, D. W., Blichert-Toft, J., Russo, C. J., Rubin, K. H., & Albarede, F. (2006). Cryptic striations  
26 in the upper mantle revealed by hafnium isotopes in southeast Indian Ridge basalts. *Nature*,  
27 440, 199–202  
28
- 29 Halpin, J. A., Crawford, A. J., Direen, N. G., Coffin, M. F., Forbes, C. J., & Borissova, I. (2008).  
30 Naturaliste Plateau, offshore Western Australia: a submarine window into Gondwana  
31 assembly and breakup. *Geology*, 36, 807–810.  
32
- 33 Hanan, B. B., Blichert-Toft, J., Hemond, C., Sayit, K., Agranier, A., Graham, D. W., & Albarède, F.  
34 (2013). Pb and Hf isotope variations along the Southeast Indian Ridge and the dynamic  
35 distribution of MORB source domains in the upper mantle. *Earth and Planetary Science*  
36 *Letters*, 375, 196–208.  
37
- 38 Hart, S., Erlank, A., & Kable, E. (1974). Sea floor basalt alteration: some chemical and Sr isotopic  
39 effects. *Contributions to Mineralogy and Petrology*, 44, 219–230.  
40
- 41 Hayes, D. E., Frakes L. A., Barrett, P. J., Burns, D. A., Chen, P.-H., Ford, A. B., Kaneps, A. G., Kemp, E.  
42 M., McCollum, D. W., Piper, D. J. W., Wall, R. E., & Webb, P. N. (1975). *Site 264, Initial Reports*  
43 *of the Deep Sea Drilling Project* (pp. 821–833). Washington DC: U.S. Government Printing  
44 Office.  
45
- 46 Heezen, B. C., & Tharp, M. (1973). USNS *Eltanin* cruise 55. *Antarctic Journal of the United States*,  
47 VIII, 137–141.  
48
- 49 Ingle, S., Scoates, J. S., Weis, D., Brugmann, G., & Kent, R. W. (2004). Origin of Cretaceous  
50 continental tholeiites in southwestern Australia and eastern India: insights from Hf and Os  
51 isotopes. *Chemical Geology*, 209, 83–106.  
52
- 53 Ingle, S., Weis, D., & Frey, F.A. (2002a). Indian continental crust recovered from Elan Bank,  
54 Kerguelen Plateau (ODP Leg 183, Site 1137). *Journal of Petrology*, 43, 1241–1257.  
55  
56  
57  
58  
59  
60

Ingle, S., Weis, D., Scoates, J. S., & Frey, F.A. (2002b). Relationship between the early Kerguelen plume and continental flood basalts of the paleo-Eastern Gondwanan margins. *Earth and Planetary Science Letters*, 197, 35–50.

Ingle, S., Weis, D., Doucet, S., & Mattielli, N. (2003). Hf isotope constraints on mantle sources and shallow-level contaminants during Kerguelen hotspot activity since 120 Ma. *Geochemistry Geophysics Geosystems*, 4, 1068 doi: 10.1029/2002GC000482.

Jongsma, D., & Petkovic, P. (1977). The structure of the Naturaliste Plateau and trough. *The APEA Journal*, 17, Part 1, 3–12.

Kent, R. W., Pringle, M. S., Müller, R. D., Saunders, A. D., & Ghose, N. C. (2002). <sup>40</sup>Ar / <sup>39</sup>Ar geochronology of the Rajmahal basalts, India and their relationship to the Kerguelen Plateau. *Journal of Petrology*, 43, 1141–1153.

Kent, R. W., Saunders, A. D., Kempton, P. D., & Ghose, N. C. (1997). Rajmahal basalts, eastern India: mantle sources and melt distribution at a volcanic rifted margin. In J. J. Mahoney & M. F. Coffin (Eds.), *Large Igneous Provinces: Continental, Oceanic and Planetary Flood Volcanism* (pp. 145–182). Washington DC: American Geophysical Union Geophysical Monograph 100.

Kent, R. W., Storey, M., & Saunders, A. D. (1992). Large igneous provinces: Sites of plume impact or plume incubation? *Geology*, 20, 891–894.

Kirkland, C., Spaggiari, C., Pawley, M., Wingate, M., Smithies, R., Howard, H., Tyler, I., Belousova, E. A., & Poujol, M. (2011). On the edge: U–Pb, Lu–Hf, and Sm–Nd data suggests reworking of the Yilgarn craton margin during formation of the Albany–Fraser Orogen. *Precambrian Research*, 187, 223–247.

Le Bas, M. J., Le Maitre, R., Streckeisen, A., & Zanettin, B. (1986). A chemical classification of volcanic rocks based on the total alkali-silica diagram. *Journal of Petrology*, 27, 745–750.

Mahoney, J. J., Jones, W. B., Frey, F. A., Salters, V. J. M., Pyle, D. G., & Davies, H. L. (1995). Geochemical characteristics of lavas from Broken Ridge, the Naturaliste Plateau and southernmost Kerguelen Plateau: Cretaceous plateau volcanism in the southeast Indian Ocean. *Chemical Geology*, 120, 315–345.

Mahoney, J. J., Graham, D. W., Christie, D. M., Johnson, K. T. M., Hall, L. S., & Vonderhaar, D. L. (2002). Between a hotspot and a cold spot: isotopic variation in the Southeast Indian Ridge asthenosphere, 86°E–118°E. *Journal of Petrology*, 43, 1155–1176.

Maloney, D., Sargent, C., Direen, N. G., Hobbs, R. W., & Grocke, D.R. (2011). Re-evaluation of the Mentelle Basin, a polyphase rifted margin basin, offshore south-west Australia: new insights from integrated regional seismic datasets. *Solid Earth*, 2, 107–123.

Markl, R. G. (1978). Further evidence for the Early Cretaceous breakup of Gondwanaland off southwestern Australia. *Marine Geology*, 26, 41–48.

McDonough, W. F., & Sun, S.-S. (1995). The composition of the Earth. *Chemical Geology*, 120, 223–253.

- Mihut, D., & Mueller, R. D. (1998). Volcanic margin formation and Mesozoic rift propagators in the Cuvier abyssal plain off Western Australia. *Journal of Geophysical Research, B, Solid Earth and Planets*, 103, 27 135–27 149.
- Mutter, J. C., & Cande, S. C. (1983). The early opening between Broken Ridge and Kerguelen Plateau. *Earth and Planetary Science Letters*, 65, 369–376.
- Neal, C. R., Mahoney, J., & Chazey, W. (2002). Mantle sources and the highly variable role of continental lithosphere in basalt petrogenesis of the Kerguelen Plateau and Broken Ridge LIP: results from ODP Leg 183. *Journal of Petrology*, 43, 1177–1205.
- Olierook, H. K., Merle, R. E., Jourdan, F., Sircombe, K., Fraser, G., Timms, N. E., Nelson, G., Dadd, K. A., Kellerson, L., & Borissova, I. (2015). Age and geochemistry of magmatism on the oceanic Wallaby Plateau and implications for the opening of the Indian Ocean. *Geology*, 43, 971–974.
- Olierook, H. K., Jourdan, F., Merle, R. E., Timms, N. E., Kuszniir, N., & Muhling, J. R. (2016). Bunbury Basalt: Gondwana breakup products or earliest vestiges of the Kerguelen mantle plume? *Earth and Planetary Science Letters*, 440, 20–32.
- Pearce, J. A. (1996). A user's guide to basalt discrimination diagrams. In D. A. Wyman (Ed.), *Trace Element Geochemistry of Volcanic Rocks: Applications for Massive Sulphide Exploration* (pp. 79–113). St John's NL Canada: Geological Association of Canada, Short Course Notes Vol. 12.
- Pearce, J. A., & Cann, J. (1973). Tectonic setting of basic volcanic rocks determined using trace element analyses. *Earth and Planetary Science Letters*, 19, 290–300.
- Pearce, J., & Norry, M. (1979). Petrogenetic implications of Ti, Zr, Y, and Nb variations in volcanic rocks. *Contributions to Mineralogy and Petrology*, 69, 33–47.
- Péron-Pinvidic, G., & Manatschal, G. (2009). The final rifting evolution at deep magma-poor passive margins from Iberia–Newfoundland: a new point of view. *International Journal of Earth Sciences*, 98, 1581–1597.
- Petkovic, P. (1975). Origin of the Naturaliste Plateau. *Nature*, 253, 30–33.
- Planke, S., Symonds, P. A., Alvestad, E., & Skogseid, J. (2000). Seismic volcanostratigraphy of large volume basaltic extrusive complexes on rifted margins. *Journal of Geophysical Research*, 105, 19 335–19 351.
- Powell, C. M., Roots, S. R., & Veevers, J. J. (1988). Pre-breakup continental extension in East Gondwanaland and the early opening of the eastern Indian Ocean. *Tectonophysics*, 155, 261–283.
- Rosman, K., Wilde, S., Libby, W., & De Laeter, J. (1980). Rb–Sr dating of granitic rocks in the Pemberton area. *Western Australian Geological Survey, Annual Report for 1979* (pp. 97–100). Perth WA: Western Australian Geological Survey.
- Royer, J. Y., & Coffin, M. F. (1992). Jurassic to Eocene plate tectonic reconstructions in the Kerguelen Plateau region. In S. W. Wise, Jr., & R. Schlich (Eds.), *Proceedings of the Ocean Drilling Program, Scientific Results v. 120*, pp. 917–928.

Rudnick, R. L., & Gao, S. (2014). 4.1 – Composition of the Continental Crust A2 – Holland, H. D, In K. K. Turekian (Ed.), *Treatise on Geochemistry (Second Edition)* (pp. 1–51). Oxford UK: Elsevier.

Sayers, J., Symonds, P. A., Direen, N. G., & Bernardel, G. (2001). Nature of the continent–ocean transition on the non-volcanic rifted margin of the central Great Australian Bight. In R. C. L. Wilson, R. B. Whitmarsh, B. Taylor & N. Froitzheim (Eds.), *Non-volcanic rifting of continental margins; a comparison of evidence from land and sea* (pp. 51–76). London UK: Geological Society (London) Special Publication 187.

Stagg, H. M. J., Colwell, J. B., Direen, N. G., O'Brien, P. E., Bernardel, G., Borissova, I., Brown, B. J., & Ishihara, T. (2004). Geology of the continental margin of Enderby and Mac. Robertson Lands, East Antarctica: Insights from a regional data set. *Marine Geophysical Researches*, 25, 183–219.

Stagg, H. M. J., Colwell, J. B., Borissova, I., Ishihara, T., & Bernardel, G. (2006). The Bruce Rise Area, East Antarctica: Formation of a Continental Margin near the Greater India–Australia–Antarctica Triple Junction. *Terra Antarctica*, 13, 3–22.

Storey, M., Kent, R. W., Saunders, A. D., Salters, V. J. M., Hergt, J., Whitechurch, H., Seigney, J. H., Thirlwall, M. F., Leat, P., Ghose, N. C., & Gifford, M. (1992). Lower Cretaceous volcanic rocks on continental margins and their relationship to the Kerguelen Plateau. In S. W. Wise, R. Schlich, et al (Eds.), *Proceedings of the Ocean Drilling Program, Scientific Results* (pp. 33–47). College Station, Texas: Ocean Drilling Program.

Tikku, A. A., & Cande, S. C. (2000). On the fit of Broken Ridge and Kerguelen Plateau. *Earth and Planetary Science Letters*, 180, 117–132.

Tikku, A. A., & Direen, N. G. (2008). Comment on “Major Australian–Antarctic Plate Reorganization at Hawaiian–Emperor Bend Time”. *Science*, 321, 490–491.

Totterdell, J., Blevin, J., Struckmeyer, H., Bradshaw, B., Colwell, J., & Kennard, J. (2000). Petroleum frontiers, systems and plays–A new sequence framework for the Great Australian Bight: Starting with a clean slate. *APPEA Journal-Australian Petroleum Production and Exploration Association*, 40, 95–120.

Turek, A., & Stephenson, N. (1966). The radiometric age of the Albany Granite and the Stirling Range Beds, southwest Australia. *Journal of the Geological Society of Australia*, 13, 449–456.

Veevers, J. J., & Li, Z. X. (1991). Review of seafloor spreading around Australia. II. Marine magnetic anomaly modelling. *Australian Journal of Earth Sciences*, 38, 391–408.

White, W., & Klein, E. (2014). 4.13-Composition of the Oceanic Crust. In K. K. Turekian (Ed.), *Treatise on Geochemistry (Second Edition)* (pp. ). Oxford UK: Elsevier.

Williams, S. E., Whittaker, J. M., Granot, R., & Mueller, R. D. (2013). Early India–Australia spreading history revealed by newly detected Mesozoic magnetic anomalies in the Perth Abyssal Plain. *Journal of Geophysical Research*, 118, 1–10.

Winchester, J., & Floyd, P. (1977). Geochemical discrimination of different magma series and their differentiation products using immobile elements. *Chemical Geology* 20, 325–343.

Zhu, D., Mo, X., Pan, G., Zhao, Z., Dong, G., Shi, Y., Liao, Z., Wang, L., & Zhou, C. (2008). Petrogenesis of the earliest Early Cretaceous mafic rocks from the Cona area of the eastern Tethyan Himalaya in south Tibet: Interaction between the incubating Kerguelen plume and the eastern Greater India lithosphere? *Lithos*, 100, 147–173.

Zhu, D.-C., Chung, S.-L., Mo, X.-X., Zhao, Z.-D., Niu, Y., Song, B., & Yang, Y.-H. (2009). The 132 Ma Comei-Bunbury large igneous province: Remnants identified in present-day southeastern Tibet and southwestern Australia. *Geology*, 37, 583–586.

# Figure and table captions

Table 1. *RV Southern Surveyor* SS09/05 Dredge location and contents.

Table 2. Abundance of major elements (wt%).

Table 3. Abundance of trace elements (ppm) analysed by X-Ray Fluorescence.

Table 4. Abundance of trace elements (ppm) analysed by ICP-MS.

Table 5. Radiogenic (Sr–Nd–Hf–Pb) isotope compositions.

Figure 1. (a) Regional tectonic setting based on bathymetry of the Indian Ocean. NP, Naturaliste Plateau; WP, Wallaby Plateau; WZFZ, Wallaby-Zenith Fracture Zone; NK, northern Kerguelen Plateau; CK, central Kerguelen Plateau; SK, southern Kerguelen Plateau; BR, Broken Ridge; R, Rajmahal Traps; C, Cona Basalts; H, Houtman Sub-Basin; V, Vlaming Sub-Basin; Z, Zeewyck Sub Basin; AAP= Argo Abyssal Plain. Map projection is American Polyconic, with the central meridian at 85° E. Scale is in meters below sea level. (b) Location map of the *R/V Southern Surveyor* voyage SS2005/09 sample locations on the Naturaliste Plateau (Crawford, 2005), regional bathymetry in metres below sea level. Blue numbered squares, dredges from this study; red circles, DSDP boreholes (Burkle et al., 1967; Ford, 1975; Hayes et al., 1975); prior dredge sites from *USNS Eltanin* (Coleman et al., 1982), yellow star; and *R/V Marion Dufresne* (Beslier et al., 2004), inverted red triangle. Map projection is Mercator, Ellipsoid WGS84.

Figure 2. Reconstructions of east Gondwana breakup. (a) 132 Ma, (b) 128 Ma, (c) 118 Ma, (d) 95 Ma, (e) 83 Ma and (f) 43 Ma (adapted from Coffin et al., 2002). Blue diamond denotes initial preferred location of Kerguelen hotspot, red polygons are outlines of LIP fragments associated with this event at 132 Ma, and subsequently. Green polygons are current continental outlines, and tan outlines delimit both extended continental crust and Continent Ocean Transition Zone regions out to the Continent Ocean Boundary, defined as the inboard limit of unambiguous oceanic crust. Abbreviations as for Figure 1, except KP, Kerguelen Plateau; CC, Comei-Cona Basalts. Map projection is Stereographic (conformal), with 105° and –90° as the viewpoint.

Figure 3. U–Pb concordia diagram for zircons from DR10-16 (granophyre), DR11-6 (monzodiorite) and DR12-29 (rhyolite). Error bars shown at 1σ for clarity, age uncertainties given at 1σ. For further details, see Supplementary Papers Appendix 3.

Figure 4. <sup>40</sup>Ar–<sup>39</sup>Ar step-heating and <sup>36</sup>Ar/<sup>40</sup>Ar vs <sup>39</sup>Ar/<sup>40</sup>Ar isochron diagrams for plagioclase separates from DR11-19 (basalt) and dolerites DR12-8 and DR13-33. Plateau age errors are calculated as the standard error of the weighted mean; if MSWD>1, errors are calculated as the standard error of the weighted mean multiplied by the square root of the MSWD; light-brown dashed lines indicate the 2σ error envelopes. Further detail, see Supplementary Papers Appendix 4.

Figure 5. Major element compositions of *RV Southern Surveyor* 2005 cruise dredge samples from the southern margin of the Naturaliste Plateau. (a) SiO<sub>2</sub> vs MgO, (b) TiO<sub>2</sub> vs MgO, (c) Total Alkali Silica. TAS, diagram (after Le Bas et al., 1986), showing effects of submarine alteration scattering the alkali oxides. Panel (d) shows the Zr/Y vs Zr/Nb variations with the alkalic–subalkaline (tholeiitic) divide (after Winchester and Floyd (1977) as modified by Pearce (1996)): this identifies almost all of the dredge samples as tholeiitic. (e, f) Initial <sup>87</sup>Sr/<sup>86</sup>Sr and εNd vs MgO and SiO<sub>2</sub>, respectively. Data for other sectors of the Naturaliste Plateau (DSDP site 264, Eltanin 1972 cruise, see Figure 1), for Cretaceous basaltic suites from the Kerguelen Plateau (KP, ODP sites 738 and 1138) and for ca130 Ma Bunbury Basalt shown for comparison. Data sources: Coleman et al. (1982), Ford (1975), Frey et al. (1996), Mahoney et al. (1995), Neal et al. (2002), Olierook et al. (2016), and Storey et al. (1992).

Figure 6. Trace element variations (a) Sr vs Ce, (b) Nb vs Ce; (c) Zr vs Ce. Panel (d) shows covariation of initial <sup>87</sup>Sr/<sup>86</sup>Sr and εNd with Zr concentration. This implies that the measured initial <sup>87</sup>Sr/<sup>86</sup>Sr are robust, despite possible alteration effects on Sr concentrations (a). Also shown are available data for DSDP Site 264 and from the Eltanin cruise, from the southern and northern Naturaliste Plateau, respectively. Data sources, see Figure 5.

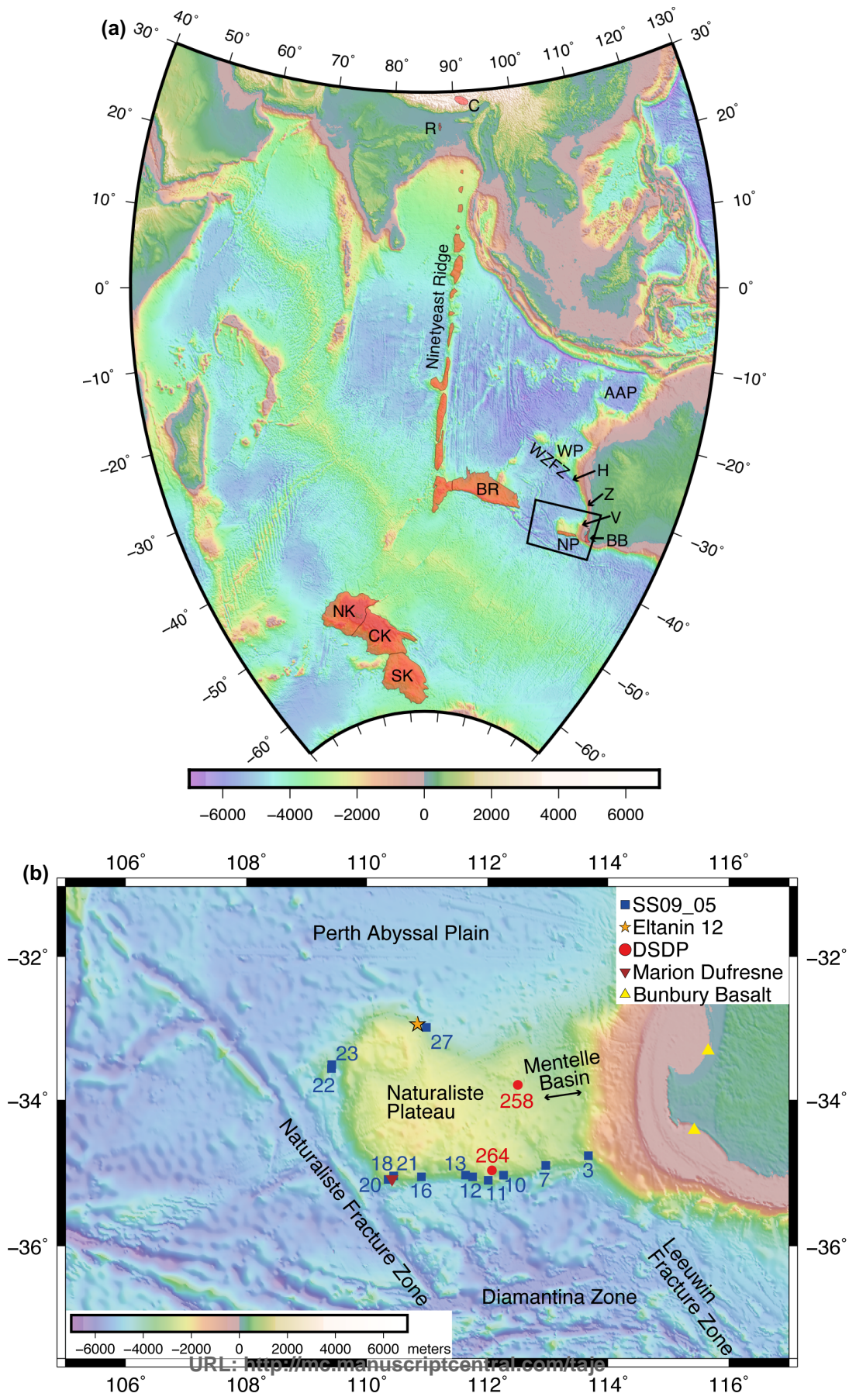
Figure 7. Rare earth element and Th/Nb vs La/Nb systematics. (a) Chondrite-normalised REE patterns for the *RV Southern Surveyor* dredge sample suite (small grey circles). Several of the patterns are highlighted: basalt DR7-11, with the highest MgO content (7.26 wt%) of the sample suite, has a MORB-like pattern; dolerites 10–39 (6.52 wt% MgO) and DR13-7 (5.35 wt% MgO) have the most juvenile Sr–Nd isotope ratios of the suite; granophyre DR10-16 and rhyolite DR12-41 have high LREE/HREE and are Eu-depleted. Eu/Eu\* correlates with MgO and Al<sub>2</sub>O<sub>3</sub> and anti-correlates with La, La/Sm and SiO<sub>2</sub> (not shown). About half of the samples have Ce anomalies (negative and positive); Ce/Ce\* shows no clear correlation with sample composition except LOI. A similar range of REE patterns was reported from undated but probably Cretaceous basalts in other sectors of the Naturaliste Plateau (Eltanin and DSDP264, grey field). (b) The range of REE patterns in Naturaliste Plateau basalts (grey field) completely overlaps that of Cretaceous basalts from the Kerguelen Plateau (ODP1138, note strongly LREE-enriched dacite) and onshore Western Australia (Bunbury Basalt). Average Indian Ocean MORB shown for comparison (from White & Klein, 2014). Chondrite REE concentrations from McDonough and Sun (1995). (c) Th/Nb vs La/Nb (normalised to primitive mantle) plot for dredged rocks (red, this study), northern Naturaliste Plateau flank (blue). Symbols for other Cretaceous basalts are: Bunbury Basalt (Casuarina and Gosselin Suites), Kerguelen Plateau (ODP Sites 738, 1137, 1138). AFO is the field for the Albany-Fraser Orogen in southern Western Australia, and UCC and LCC are fields for

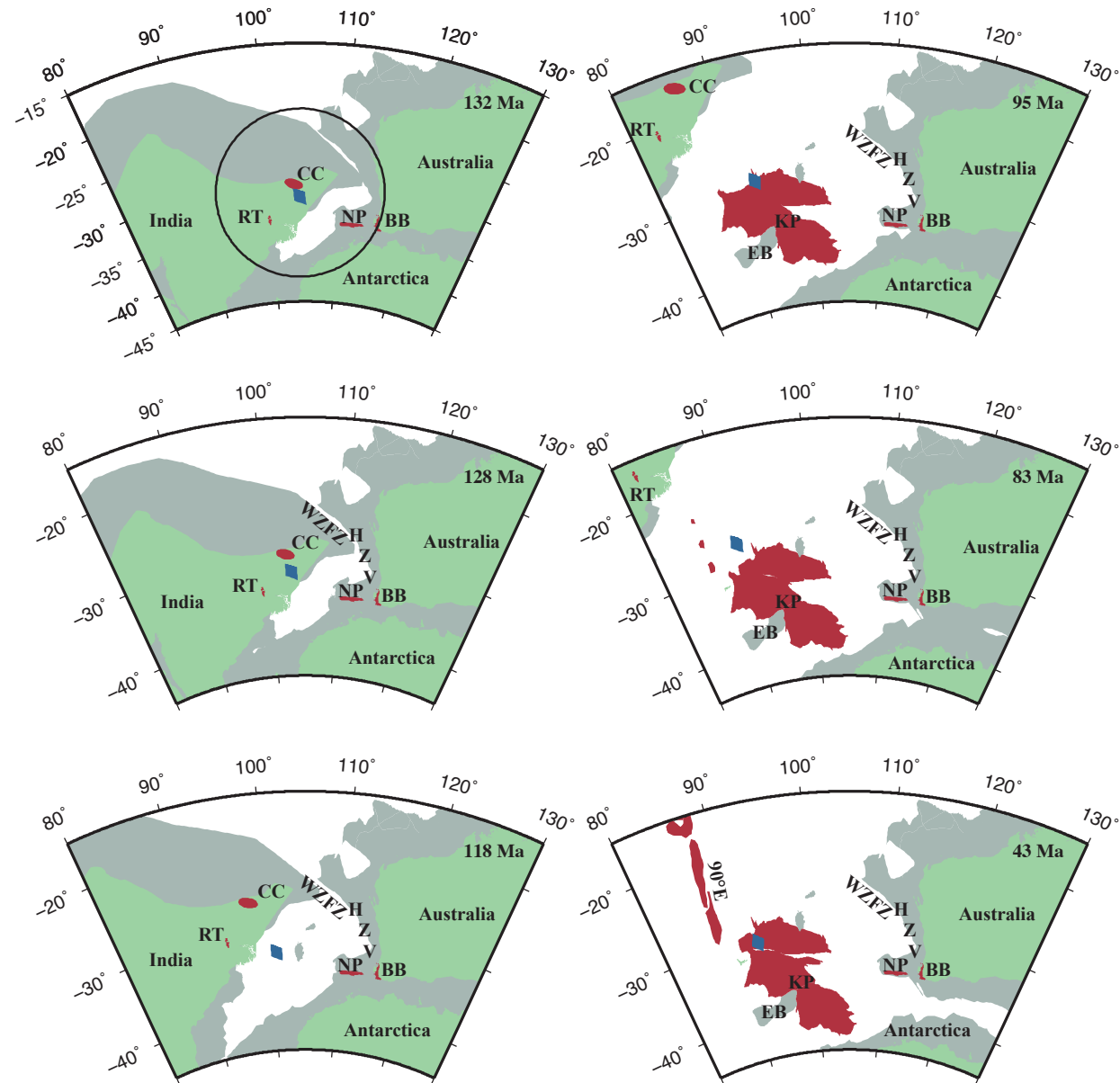
various averages and sample suites representing the upper and lower continental crust, respectively. Data sources: Fitton et al. (2000), Frey et al. (1996), Mahoney et al. (1995), Neal et al. (2002), Rudnick & Gao (2104), Storey et al. (1992), and references therein; AFO data based on Geological Survey of Western Australia (Hugh Smithies unpubl. data).

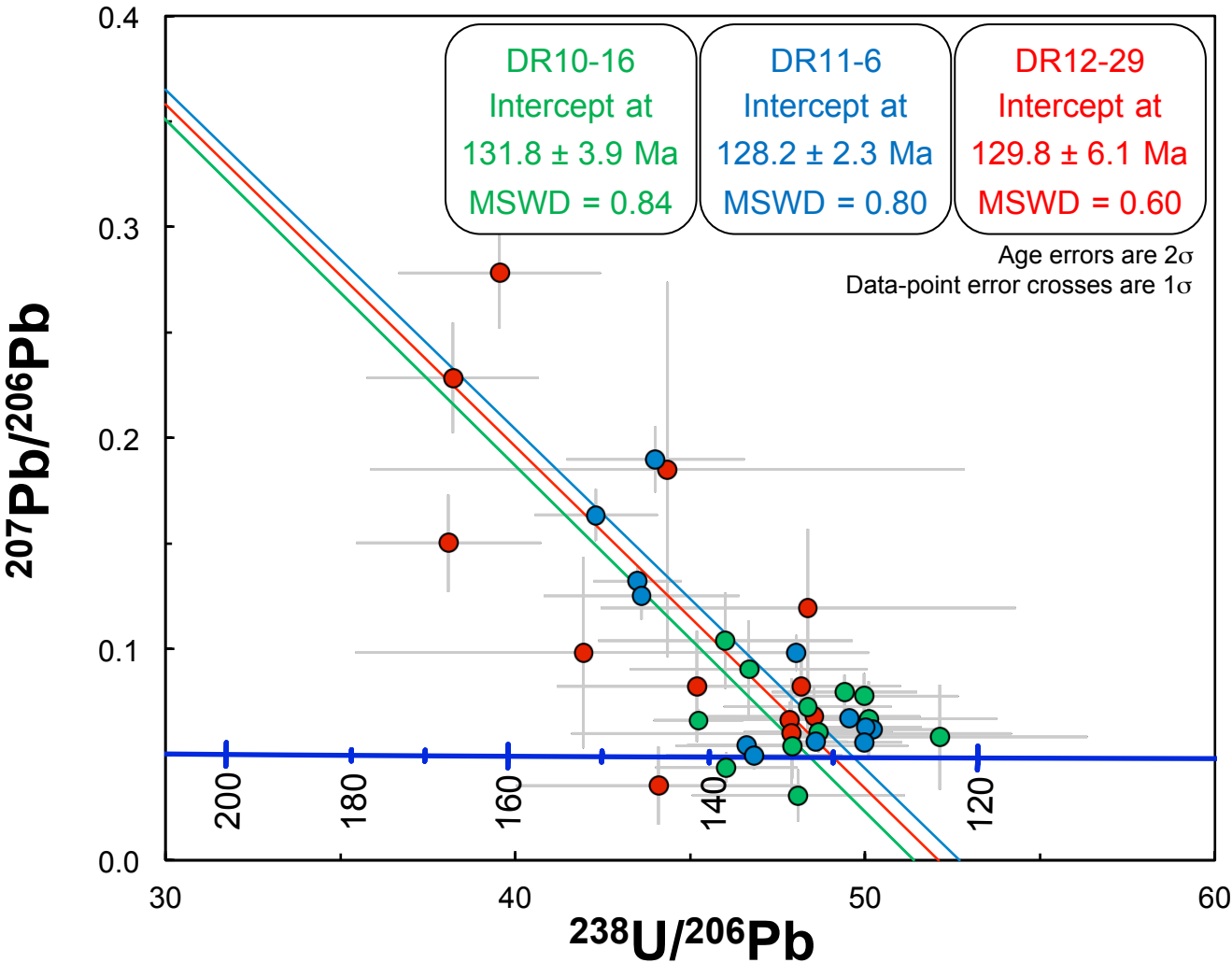
Figure 8. Sr–Nd–Pb–Hf isotope variations for Naturaliste Plateau dredge samples ('SNP basalts'), calculated at 130 Ma. Also shown are data for basalts from other sites on the northern Naturaliste Plateau ('NNP'), Bunbury Basalt, Rajmahal Traps, Broken Ridge, Cretaceous basalts from various ODP sites on the Kerguelen Plateau ('KP'), and modern MORB from the SE Indian Ridge ('SEIR'). (a) Sr–Nd isotopes, binary mixing lines drawn between a mantle endmember (300 ppm Sr,  $^{87}\text{Sr}/^{86}\text{Sr}$  0.7028, 10 ppm Nd,  $^{143}\text{Nd}/^{144}\text{Nd}$  0.51295,  $\epsilon\text{Nd}$  +9.5) and two crustal endmembers modelled on data for the Albany Fraser Orogen (100 ppm Sr, 0.740, 40 ppm Nd, 0.51149, –19; 150 ppm Sr, 0.740, 20 ppm Nd, –19). (b) Hf–Nd isotopes, mixing lines are for two similar mantle endmembers (1–2 ppm Hf,  $^{176}\text{Hf}/^{177}\text{Hf}$  0.28315,  $\epsilon\text{Hf}$  +15.8, 10 ppm Nd,  $^{143}\text{Nd}/^{144}\text{Nd}$  0.51295,  $\epsilon\text{Nd}$  +9.5) and two similar crustal endmembers modelled on data for the Albany Fraser Orogen (4–5 ppm Hf,  $^{176}\text{Hf}/^{177}\text{Hf}$  0.282135,  $\epsilon\text{Hf}$  –20.1, 30 ppm Nd,  $^{143}\text{Nd}/^{144}\text{Nd}$  0.51149,  $\epsilon\text{Nd}$  –19.0). (c)  $^{207}\text{Pb}/^{204}\text{Pb}$  vs  $^{206}\text{Pb}/^{204}\text{Pb}$ . (d)  $^{208}\text{Pb}/^{204}\text{Pb}$  vs  $^{206}\text{Pb}/^{204}\text{Pb}$ . Data sources: Davies et al. (1989), Frey et al. (1996, 2002), Graham, Blichert-Toft, Russo, Rubin, & Albarede (2006), Hanan et al. (2013), Ingle et al. (2002, 2003, 2004), Kent et al. (1997), Mahoney et al. (1995, 2002), Neal et al. (2002), Storey et al. (1992) and dredged gneisses from the southern Naturaliste Plateau (orange squares, R. Maas unpubl. data).

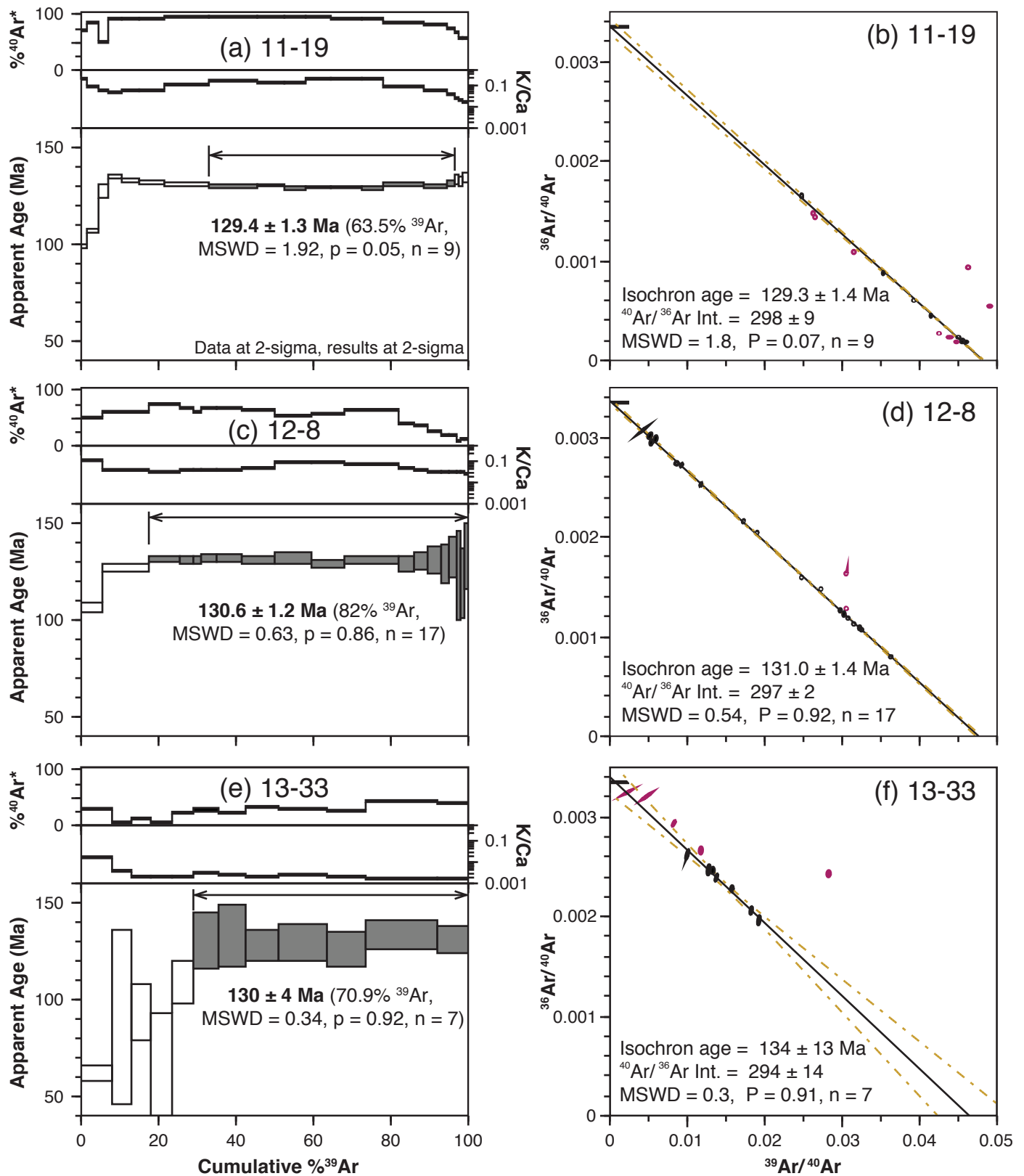
Figure 9. Hf–Pb and Pb–Pb isotope variations for Naturaliste Plateau dredge samples ('SNP basalts'), at 130 Ma. Also shown are data for basalts from other sites on the Naturaliste Plateau, Bunbury Basalt, Rajmahal Traps, Broken Ridge, Cretaceous basalts from various ODP sites on the Kerguelen Plateau, and modern MORB from the SE Indian Ridge (see Figure 8). Various inferred source components (Plume Head, Lower Crust, Upper Crust) inferred to be involved in the Cretaceous Kerguelen LIP and Naturaliste Plateau basalts (loosely modelled after Ingle et al., 2003) are shown for reference.

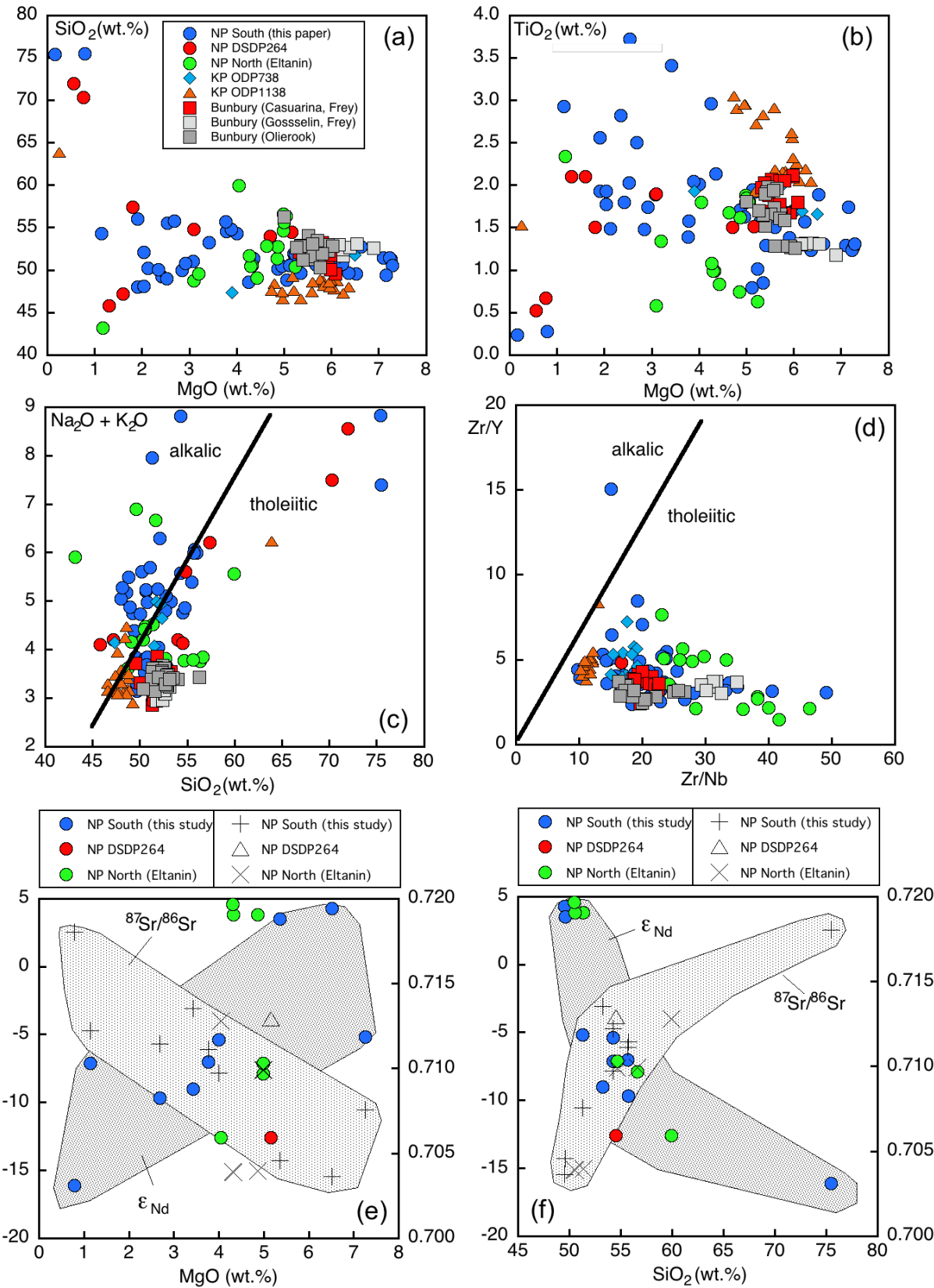




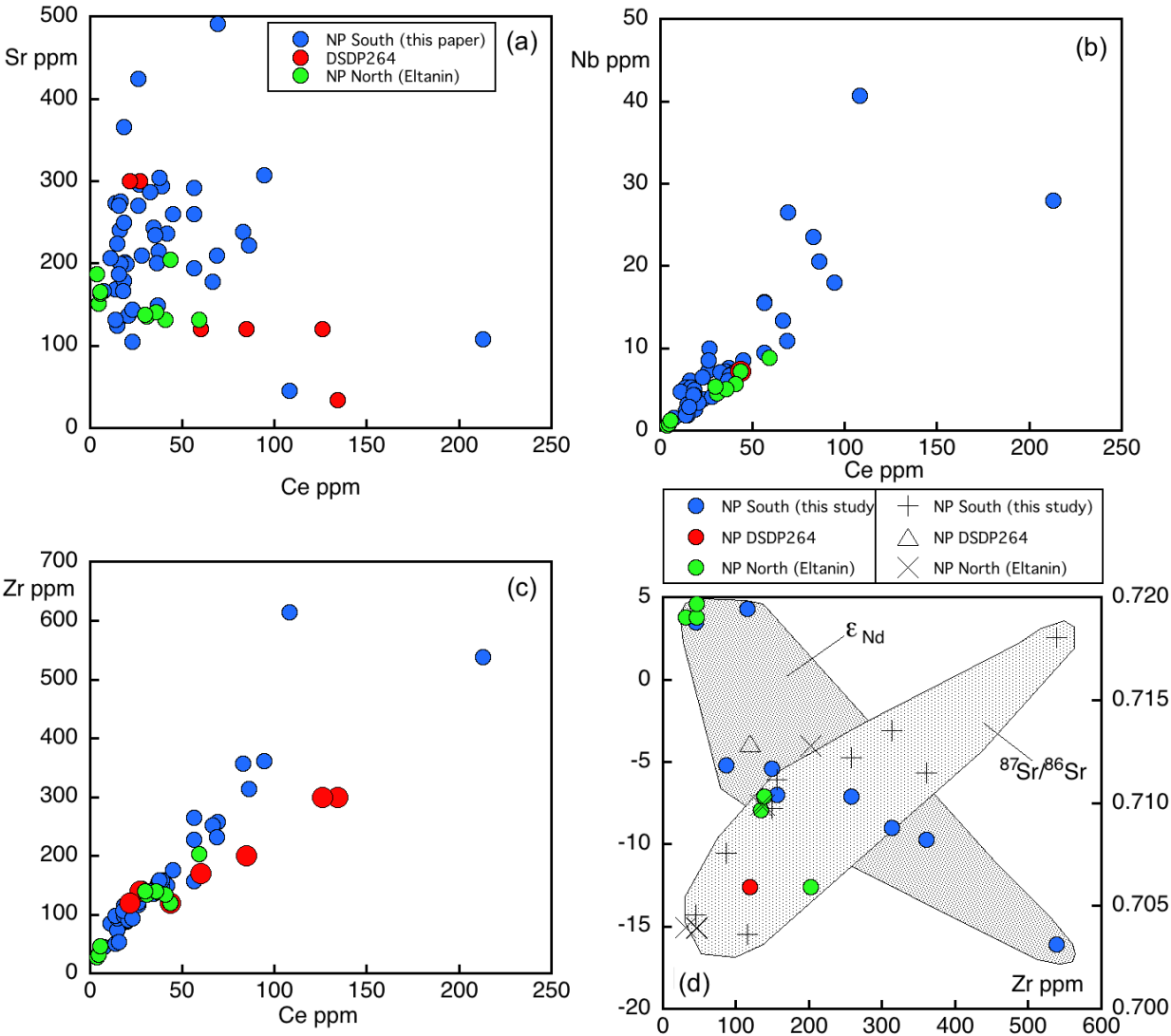




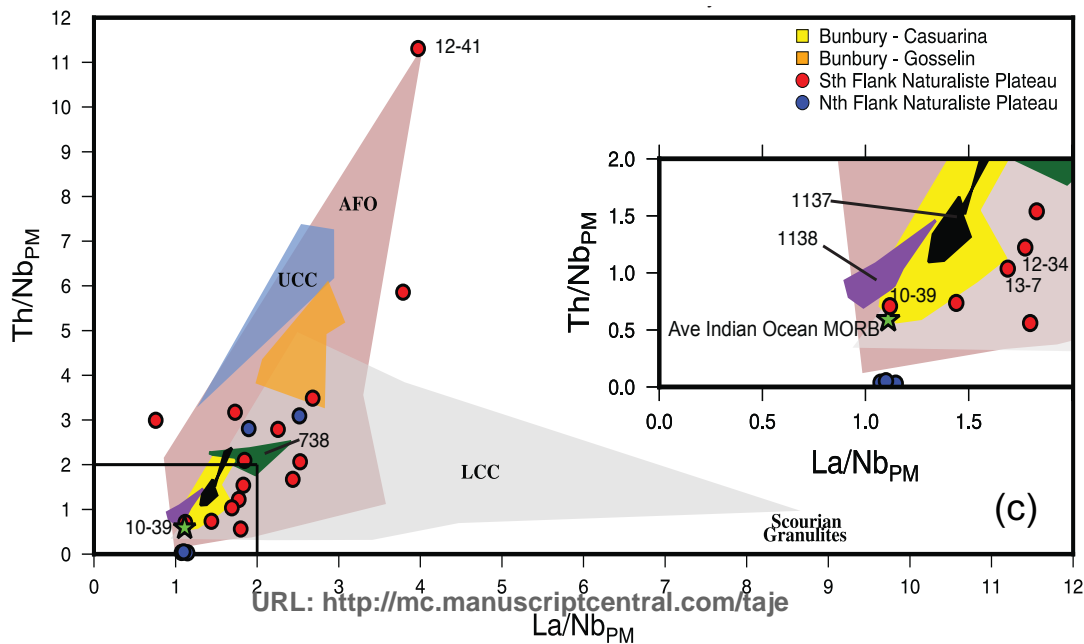
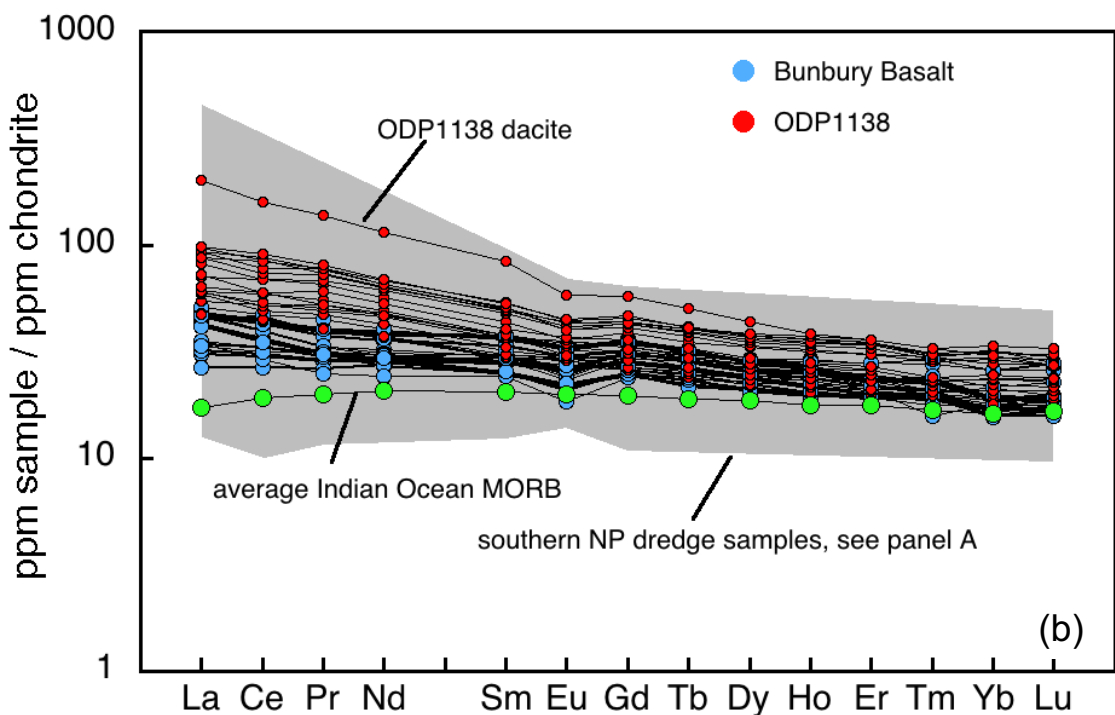
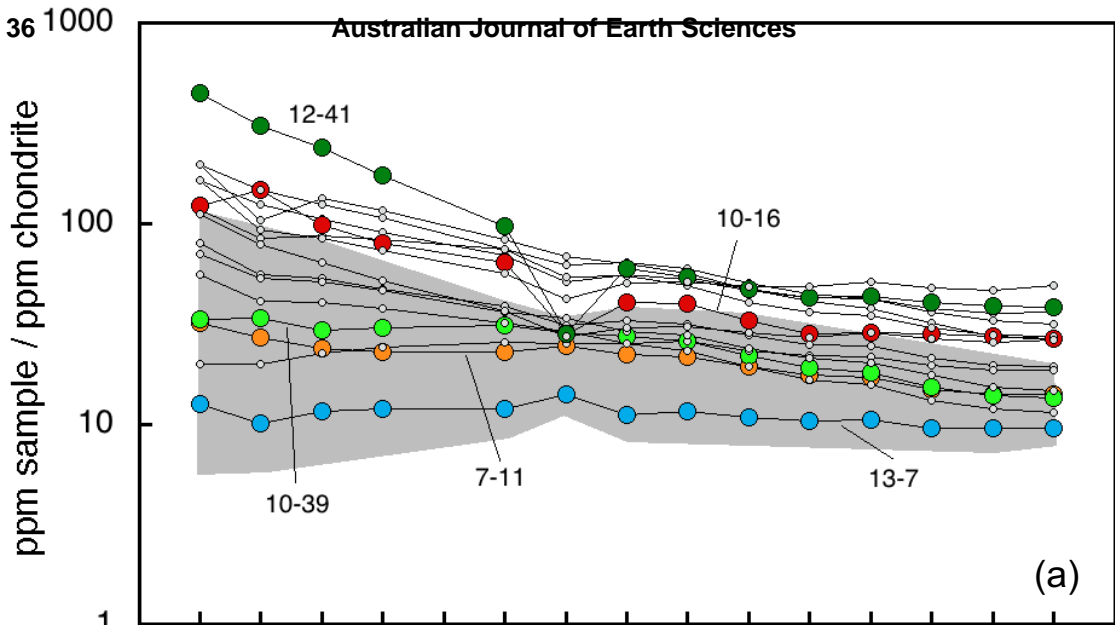


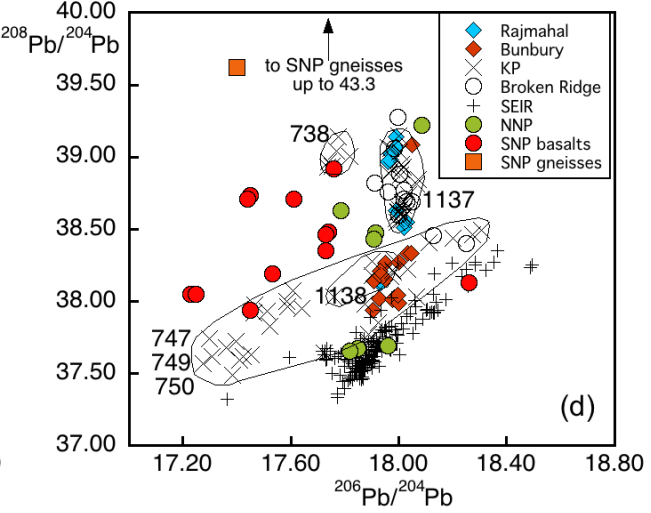
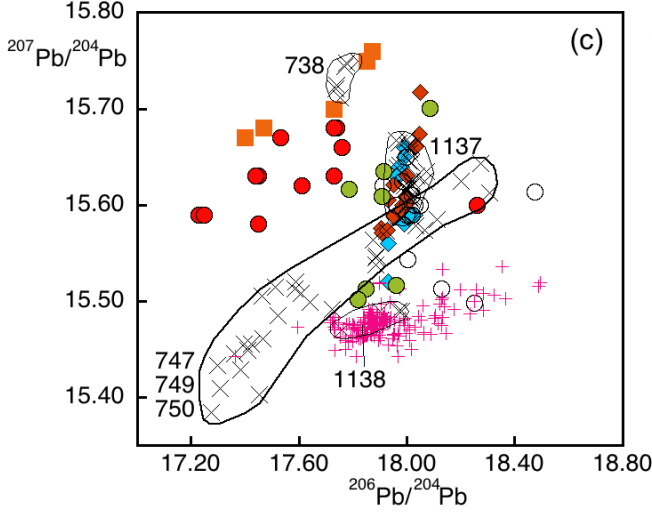
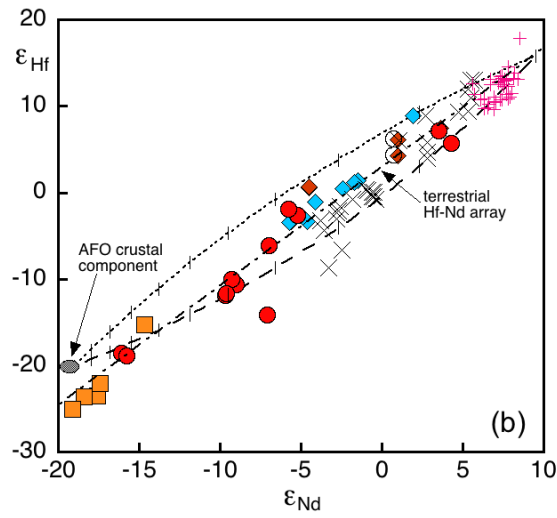
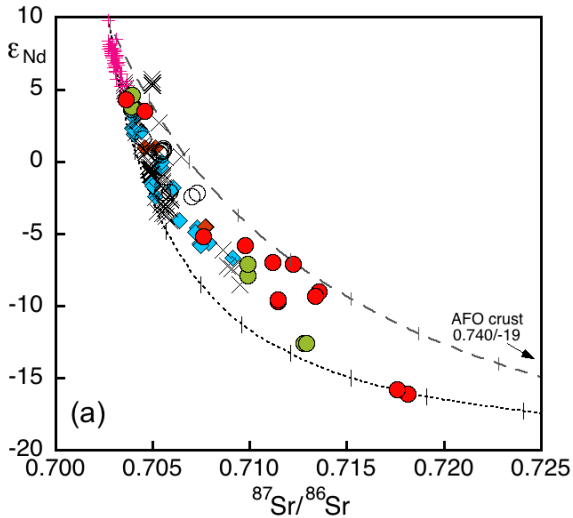






1  
2  
3  
4  
5  
6  
7  
8  
9  
10  
11  
12  
13  
14  
15  
16  
17  
18  
19  
20  
21  
22  
23  
24  
25  
26  
27  
28  
29  
30  
31  
32  
33  
34  
35  
36  
37  
38  
39  
40  
41  
42  
43  
44  
45  
46  
47  
48  
49  
50  
51  
52  
53  
54  
55  
56  
57  
58  
59  
60







1  
2  
3  
4  
5  
6  
7  
8  
9  
10  
11  
12  
13  
14  
15  
16  
17  
18  
19  
20  
21  
22  
23  
24  
25  
26  
27  
28  
29  
30  
31  
32  
33  
34  
35  
36  
37  
38  
39  
40  
41  
42  
43  
44  
45  
46  
47  
48  
49  
50  
51  
52  
53  
54  
55  
56  
57  
58  
59  
60

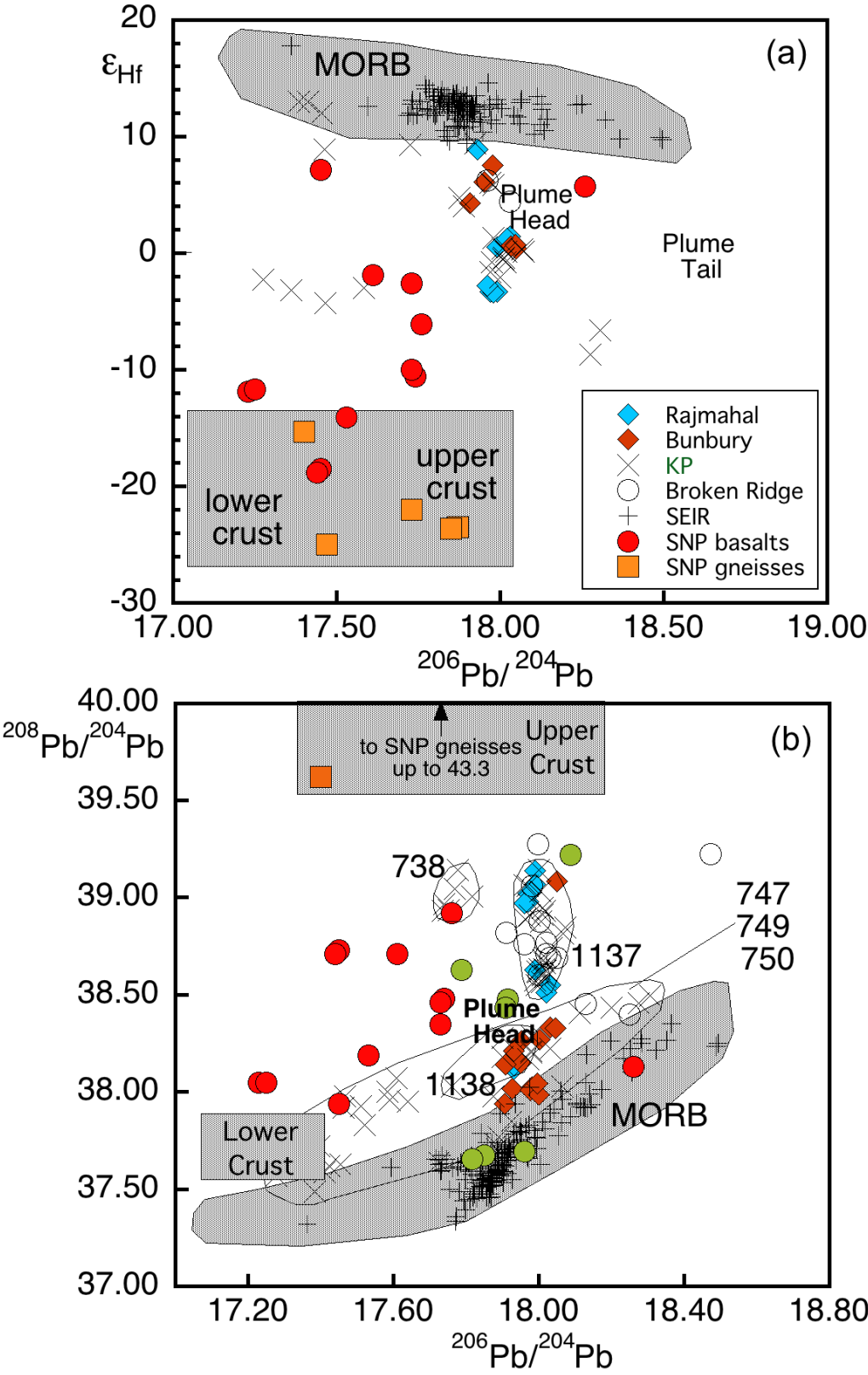


Table 1. *RV Southern Surveyor* SS09/05 Dredge location and contents.

Station#	Locality	Start Lat.	Start Long.	End Lat.	End Long.	Depth Start	Depth End	Total Weight	Dredge haul description
DR3	Seamount at NW end of Leeuwin Escarpment	−34.7698	113.6449	−34.7664	113.6519	3851	3690	20 kg	Cobbles of metasediments and volcanics plus several white muddy limestone cobbles
DR7	South-facing scarp, south margin NP	−34.9021	112.9389	−34.8697	112.9424	3710	3200	100+ kg	Altered vesicular mafic lavas, felsic lavas
DR10	South-facing scarp, south margin NP	−35.0356	112.2374	−35.0358	112.2115	3752	3072	500 kg	Coarse qtz-poor felsic intrusive (altered) + abundant altered mafic lavas, intrusives and lava breccia
DR11	South-facing scarp, south margin NP	−35.1058	111.9827	−35.0969	111.9830	3600	3180	500 kg	Angular blocks granodiorite, altered mafic lavas and lava breccia
DR12	South-facing scarp, south margin NP	−35.0586	111.7235	−35.0393	111.7251	3700	3250	500 kg	Altered mafic volcanics, felsic lavas
DR13	South-facing scarp, south margin NP	−35.0349	111.6074	−35.0074	111.6140	3800	3130	500 kg	Altered volcanics
DR16	South-facing scarp, south margin NP	−35.0592	110.8759	−35.0577	110.8788	4140	3120	200 kg	Weathered and altered mafic volcanics
DR20	South-facing scarp, south margin NP	−35.0943	110.3241	−35.0908	110.3060	3850	3325	5 kg	Altered mafic volcanics
DR21	South-facing scarp, south margin NP	−35.0459	110.4159	−35.0410	110.4165	3900	3100	5 kg in pipe dredge	Gneiss fragments

1  
2  
3  
4  
5  
6  
7  
8  
9  
10  
11  
12  
13  
14  
15  
16  
17  
18  
19  
20  
21  
22  
23  
24  
25  
26  
27  
28  
29  
30  
31  
32  
33  
34  
35  
36  
37  
38  
39  
40  
41  
42  
43  
44  
45  
46  
47  
48  
49

Table 2. Abundance of major elements (wt%).

Dredge #	Sample description	SiO <sub>2</sub>	TiO <sub>2</sub>	Al <sub>2</sub> O <sub>3</sub>	Fe <sub>2</sub> O <sub>3</sub>	MnO	MgO	CaO	Na <sub>2</sub> O	K <sub>2</sub> O	P <sub>2</sub> O <sub>5</sub>	Loss inc S <sup>-</sup>	Total
3-2	Plagioclase-phyric, slightly vesicular basalt	54.28	2.93	18.56	8.71	0.08	1.14	4.81	3.47	5.33	0.67	2.67	99.66
3-3	Plagioclase-phyric dolerite	49.22	1.80	18.56	12.48	0.08	2.42	10.31	3.38	1.37	0.38	7.25	100.07
3-5	Altered glassy plagioclase-phyric basalt	52.12	1.77	19.66	12.20	0.08	2.03	5.55	3.30	2.99	0.29	6.78	99.74
3-7	Plagioclase-phyric basalt	50.18	1.49	20.76	13.17	0.06	2.13	6.43	3.26	2.33	0.18	6.28	99.74
7-2	Olivine-bearing dolerite	55.50	3.72	14.83	11.89	0.12	2.54	5.51	3.30	2.09	0.50	3.17	99.66
7-5	Olivine-bearing dolerite	53.23	3.41	13.27	14.02	0.17	3.42	7.05	2.99	2.00	0.45	2.38	100.46
7-10	Plagioclase-phyric basalt	51.41	1.29	17.45	9.62	0.11	7.10	9.14	3.40	0.34	0.12	3.63	99.75
7-11	Plagioclase-phyric basalt, relatively unaltered	51.27	1.27	17.00	10.10	0.14	7.26	9.33	3.18	0.31	0.13	2.55	99.85
7-28	Plagioclase-phyric basalt, moderate alteration	51.47	1.23	17.08	9.93	0.11	7.23	9.30	3.21	0.31	0.12	2.69	99.95
10-5	Plagioclase- and clinopyroxene-phyric basalt, slightly vesicular	50.01	2.82	15.40	16.52	0.25	2.35	7.08	3.77	0.97	0.84	4.85	100.14
10-14	Gabbro	49.96	1.48	21.76	8.71	0.14	2.85	10.53	3.37	0.86	0.34	2.23	99.94
10-16	Granophyre	75.39	0.24	12.39	2.81	0.03	0.16	0.12	3.86	4.98	0.03	0.82	100.11
10-39	Dolerite	49.54	1.89	15.13	13.12	0.28	6.52	9.42	3.20	0.64	0.26	2.77	99.70
10-67	Aphyric basalt	50.10	1.71	17.72	11.49	0.10	4.87	9.43	3.30	1.07	0.22	5.38	99.74
10-104	Very plagioclase phyric, vesicular basalt	54.52	1.58	19.35	8.70	0.13	3.79	6.90	3.45	1.31	0.29	6.10	100.05
11-8	Dolerite, quite altered	50.54	1.31	17.13	10.88	0.15	7.29	8.72	3.37	0.44	0.17	3.11	100.26
11-9	Coarsely plagioclase-phyric basalt	55.75	2.50	14.49	12.97	0.12	2.68	4.87	3.16	2.90	0.56	2.08	100.15
11-19	Plagioclase+clinopyroxene (both fresh) and altered olivine-phyric basalt or microdolerite	52.10	1.56	15.51	11.32	0.16	5.28	10.34	3.09	0.49	0.15	1.20	99.92
11-20	Dolerite	51.92	1.94	14.74	12.56	0.17	5.21	9.20	3.44	0.60	0.22	1.50	100.24
11-25	Dolerite	49.37	1.74	16.81	11.87	0.15	7.16	8.23	3.62	0.77	0.27	2.96	100.00
12-1	Plagioclase phyric, slightly altered basalt	49.65	1.23	14.99	12.92	0.20	6.36	11.35	2.52	0.63	0.14	1.61	100.46
12-3	Plagioclase- and clinopyroxene-phyric dolerite, moderately altered	52.73	1.31	14.24	12.10	0.16	6.63	7.55	2.47	2.64	0.16	3.47	100.57
12-17	Plagioclase-phyric, altered basalt	51.37	2.13	16.31	14.21	0.15	4.36	7.41	2.84	0.91	0.30	4.62	99.81
12-18	Aphyric basalt	48.57	2.96	16.08	17.28	0.22	4.26	4.88	3.88	1.29	0.56	5.67	99.94
12-20	Aphyric altered basalt with fresh clinopyroxene	54.27	2.01	15.43	12.15	0.16	4.00	6.12	2.90	2.68	0.27	3.82	99.71

<b>12-34</b>	Massive plagioclase- and olivine-phyric basalt	50.62	1.61	14.85	12.93	0.19	5.68	10.78	2.82	0.36	0.16	1.15	99.95
<b>12-38</b>	Plagioclase-phyric basalt	48.95	2.03	18.16	15.97	0.22	2.52	6.55	2.96	1.91	0.73	5.65	99.71
<b>12-41</b>	Rhyolite, altered glass, quartz–K-feldspar-phyric	75.47	0.28	12.10	2.90	0.05	0.79	0.90	3.36	4.04	0.11	1.90	99.68
<b>12-53</b>	Olivine- and plagioclase-phyric, very altered basalt	54.76	2.04	15.36	13.84	0.14	3.88	4.81	2.98	1.88	0.32	5.18	99.92
<b>13-1</b>	Plagioclase-phyric, altered basalt	52.72	1.50	14.46	13.16	0.17	5.60	7.39	3.16	1.64	0.20	6.56	100.55
<b>13-7</b>	Plagioclase-phyric dolerite	49.61	0.85	21.10	7.71	0.09	5.35	11.87	2.88	0.43	0.09	2.89	100.41
<b>13-34</b>	Plagioclase- and olivine-phyric basalt	51.28	1.70	16.89	12.36	0.17	6.00	3.45	4.21	3.74	0.20	7.11	99.96
<b>13-36</b>	Vesicular basalt with zeolites	48.81	1.81	18.24	13.02	0.09	5.06	7.20	3.72	1.77	0.27	4.81	99.67
<b>13-47</b>	Aphyric, slightly vesicular basalt	50.80	1.38	15.15	12.94	0.15	5.91	9.66	2.95	0.91	0.17	3.93	99.91
<b>13-51</b>	Clay-altered plagioclase-phyric basalt	51.05	1.89	17.42	13.31	0.16	3.08	6.90	3.19	2.50	0.50	5.76	100.29
<b>13-52</b>	Clay-altered plagioclase-phyric basalt	50.64	1.92	18.59	10.53	0.10	5.17	7.61	3.74	1.46	0.24	4.29	99.67
<b>13-56</b>	Plagioclase, clinopyroxene, altered olivine gabbro–dolerite	50.77	1.74	18.78	10.83	0.10	2.92	9.63	3.38	1.59	0.26	2.39	99.94
<b>13-61</b>	Large vesicular basalt	50.70	1.57	14.22	13.67	0.20	6.23	9.57	2.78	0.92	0.14	3.21	100.47
<b>13-62</b>	Plagioclase and altered olivine gabbro	50.61	1.95	18.83	10.09	0.09	5.13	7.80	3.71	1.53	0.25	3.94	99.94
<b>16-2</b>	Plagioclase-phyric vesicular basalt	55.99	1.93	14.48	14.47	0.16	1.90	4.59	2.90	3.10	0.50	3.97	99.90
<b>16-9</b>	Clinopyroxene- and plagioclase-phyric gabbro	48.01	2.56	17.57	16.32	0.22	1.91	7.02	3.60	1.46	1.34	6.41	99.83
<b>16-10</b>	Clinopyroxene- and plagioclase-phyric gabbro	50.53	0.79	18.27	10.70	0.16	5.12	9.90	2.79	1.62	0.11	3.72	99.75
<b>20-1</b>	Plagioclase- and clinopyroxene-phyric, segregation vesicles	55.66	1.39	13.29	12.79	0.16	3.77	6.74	3.53	2.46	0.22	2.54	99.99
<b>20-8</b>	Plagioclase-phyric, altered basalt	51.86	1.01	16.27	12.65	0.21	5.23	7.36	4.00	1.25	0.18	3.62	99.86
<b>21-15</b>	Moderately altered gabbro	48.13	1.93	17.11	19.11	0.24	2.03	5.83	2.79	2.49	0.33	5.63	99.73
<b>21-17</b>	Dolerite	51.74	1.29	14.54	13.75	0.16	5.41	9.42	2.77	0.75	0.16	2.12	99.51

Table 3. Abundance of trace elements (ppm) analysed by X-Ray Fluorescence.

Dredge #	Rb	Sr	Ba	Sc	Cr	V	Ni	Cu	Zn	Zr	Nb	Y	Ce
3-2	89.9	491	1250	34.8	20.6	270	11.1	20.0	163	258	26.5	58.7	69.3
3-3	17.8	260	405	39.1	162	251	25.2	31.7	149	227	9.5	41.5	56.3
3-5	43.7	296	511	40.1	109	139	44.8	63.1	145	137	10.0	25.7	26.6
3-7	43.8	241	269	40.4	187	154	59.6	39.3	158	89.5	6.1	18.0	16.0
7-2	50.9	239	644	42.5	27.0	352	23.7	26.9	105	357	23.5	55.4	83.2
7-5	50.5	222	636	31.9	25.6	311	16.0	26.3	153	314	20.6	61.5	86.1
7-10	1.7	201	102	30.4	304	188	56.1	34.4	118	87.9	2.6	24.2	18.7
7-11	1.6	199	102	31.1	294	188	51.9	28.6	118	87.4	3.8	25.2	19.6
7-28	2.1	199	97.2	29.4	298	184	51.3	27.8	104	84.1	3.6	24.3	16.5
10-5	13.0	292	198	36.9	26.9	173	37.1	71.8	223	265	15.6	64.9	56.3
10-14	12.2	366	80	24.3	54.6	164	44.2	90.7	95.2	87.7	4.5	33.9	18.4
10-16	138	45.1	592	<2	2.7	19.2	5.6	11.9	81.4	614	40.7	40.8	108
10-39	10.4	270	113	32.6	144	245	79.8	87.6	125	116	7.3	28.6	26.2
10-67	22.9	274	36	37.8	350	224	68.4	112	325	85.5	5.2	24.0	13.7
10-104	54.9	275	58.5	36.9	306	194	77.1	129	254	85.7	5.2	24.3	16.4
11-8	8.5	270	141	29.2	234	196	84.3	44.0	159	82.1	3.8	20.8	15.6
11-9	75.5	307	961	29.5	11.5	234	26.2	26.7	174	361	18.0	51.0	94.4
11-19	12.7	207	196	39.8	205	274	51.2	110	106	84.4	4.7	28.0	11.1
11-20	27.3	250	70.1	37.8	318	286	46.5	71.6	111	115	4.9	31.4	18.4
11-25	15.9	424	247	27.8	81.6	189	77.9	33.6	131	121	8.5	24.5	26.4
12-1	19.2	124	79	49.0	255	345	105	143	98.8	73.3	3.2	28.7	14.6
12-3	104	224	306	41.2	174	259	77.7	107	127	93.4	1.9	30.3	14.7
12-8	29.9	105	129	53.6	96.1	402	72.4	168	118	126	3.8	39.6	22.8
12-17	20.3	215	103	42.3	206	247	70.0	96.5	155	156	7.6	37.4	37.0
12-18	23.9	178	123	42.1	64.2	357	107	125	275	252	13.4	59.8	66.6
12-20	71.5	236	329	39.6	198	248	72.4	85.1	154	150	7.3	35.4	42.0
12-34	8.7	169	32.3	49.3	195	348	61.6	135	114	97.3	2.4	30.8	14.0
12-38	39.5	210	152	55.0	159	296	120	264	252	144	4.1	42.3	28.2
12-41	125	108	809	2.2	1.9	20.3	32.2	26.1	103	539	28.0	63.7	213
12-53	50.8	200	310	38.5	174	202	89.5	110	203	149	6.7	35.5	36.1
13-1	15.3	179	102	44.2	99.7	279	45.3	135	113	98.2	4.3	30.9	18.3
13-7	12.1	167	51.3	42.8	228	252	66.9	94.9	90.4	45	1.6	15.0	7.49
13-34	58.0	244	533	23.1	61.1	152	70.9	53.5	115	135	5.3	31.1	34.6
13-36	96.1	294	347	25.6	59.6	192	77.9	55.2	148	147	7.0	33.9	39.0
13-47	20.8	137	64.3	57.0	82.5	361	55.1	141	141	90.9	3.4	33.7	20.6
13-51	73.0	234	236	38.4	103	168	75.0	110	184	142	7.2	39.8	35.4
13-52	25.8	294	374	24.7	65.9	175	68.5	49.3	127	159	6.9	30.7	39.1
13-56	28.6	287	360	35.6	113	261	42.3	44.3	54.3	139	7.1	28.4	32.6
13-61	14.5	167	100	46.8	112	341	43.2	93.0	110	106	4.3	31.6	18.0
13-62	26.3	304	386	26.7	65.0	182	65.5	50.9	108	159	6.7	31.3	37.6
16-2	68.8	260	310	46.4	35.6	368	48.2	121	181	175	8.5	42.8	44.8
16-9	21.2	210	261	64.6	35.6	509	67.4	160	268	232	10.9	81.0	68.7
16-10	57.4	132	122	47.6	134	272	83.0	131	144	50.7	1.9	19.2	14.0
20-1	71.5	194	463	36.6	33.5	330	30.8	67.2	98.4	157	15.5	40.0	56.4
20-8	37.1	187	233	51.3	154	294	93.7	153	118	53.1	2.9	22.3	15.5
21-15	52.2	149	248	70.7	121	562	106	107	242	138	6.1	40.6	36.8
21-17	20.0	144	228	51.0	71.2	387	44.0	80.1	116	93.9	6.5	26.2	23.2

Table 4. Abundance of trace elements (ppm) analysed by ICP-MS.

Dredge #	Li	Be	Rb	Sr	Ba	Sc	V	Cr	Co	Ni	Cu	Zn	Ga	Y	Zr	Hf	Nb	Ta	Pb	U	Th
<b>3-2</b>	10.1	1.26	85.6	478	1150	29.8	249	19.8	46.9	9.05	18.6	166	29.0	60.7	250	6.35	26.2	1.75	10.9	0.716	1.78
<b>7-5</b>	10.9	1.42	50.2	213	536	34.4	293	25.3	75.6	14.2	25.4	162	23.6	63.9	318	7.90	21.3	1.54	13.0	0.857	5.40
<b>7-11</b>	24.3	0.44	1.95	191	89.5	27.6	175	267	64.1	49.5	25.3	113	20.5	25.8	88.1	2.32	3.42	0.288	4.26	0.228	1.15
<b>10-5</b>	14.8	1.04	13.4	280	174	31.4	149	21.9	50.6	33.8	68.5	219	27.3	67.7	265	7.01	15.5	1.10	3.94	0.493	2.89
<b>10-16</b>	–	7.28	138	41.9	538	3.2	1.42	16.2	1.46	90.8	13.0	102	29.0	40.9	224	7.51	39.2	3.34	10.3	1.21	14.2
<b>10-39</b>	13.1	0.86	10.3	253	92.4	35.2	248	144	73.8	69.3	81.0	124	21.1	28.4	78.2	2.20	7.17	0.563	4.23	0.227	0.614
<b>11-9</b>	20.5	1.53	77.3	290	879	24.0	201	9.21	47.7	21.9	24.3	172	24.4	53.8	326	8.14	19.4	1.34	15.9	0.555	3.93
<b>11-25</b>	41.8	0.77	15.8	409	231	26.9	179	75.9	63.4	72.0	29.9	126	20.5	25.0	64.6	2.10	9.28	0.67	3.88	0.269	0.827
<b>12-20</b>	22.1	0.87	71.8	224	292	35.8	226	182	54.6	67.3	85.8	149	19.1	37.7	147	3.81	7.21	0.528	4.61	0.444	3.04
<b>12-34</b>	11.7	0.50	9.11	165	30.5	48.3	325	188	73.4	57.6	136	118	20.2	32.8	98	2.65	2.7	0.30	0.887	0.41	0.40
<b>12-41</b>	17.6	2.86	129	103	793	3.5	17.7	1.14	42.7	30.5	27.4	105	14.9	66.1	404	11.5	27.0	1.98	30.3	2.21	36.9
<b>13-7</b>	38.1	0.27	12.1	158	41.2	37.5	222	220	70.4	63.2	88.7	95.2	18.1	15.2	43.4	1.21	1.79	0.173	0.455	0.151	0.224
<b>13-52</b>	54.1	0.80	26.5	281	329	26.1	171	65.5	54.3	65.1	48.6	133	22.4	32.0	157	3.96	6.68	0.485	4.88	0.292	1.67
<b>16-9</b>	30.9	1.24	22.1	199	226	54.7	434	31.1	74.5	63.6	162	269	27.2	85.2	229	6.11	10.4	0.691	12.2	2.07	7.36
<b>20-1</b>	11.9	0.77	71.1	182	427	38.3	298	29.5	62.4	28.4	65.0	100	18.6	41.3	153	4.01	15.5	0.82	7.14	0.691	5.95

Isotope compositions, with replicates after low-pressure (LP) and high-pressure (HP) dissolution										
1	7-5 HP	7-11	10-39	11-9 LP	11-9 HP	12-20	12-41 LP	12-41 HP	13-7	20-1
2	dolerite	basalt	dol/gabb	basalt	basalt	dolerite	rhyolite	rhyolite	dolerite	basalt
3	53.23	51.27	49.54	55.75	55.75	54.27	75.47	75.47	49.61	55.66
4	3.42	7.26	6.52	2.68	2.68	4.00	0.79	0.79	5.35	3.77
5	50.2	1.99	10.34	77.3	77.3	71.9	129.2	129.2	12.12	71.1
6	213.0	191.2	253.4	290.0	290.0	224.1	102.6	102.6	158.5	181.7
7	0.683	0.03	0.118	0.772	0.772	0.928	3.65	3.65	0.221	1.132
8	0.714607	0.707639	0.70383	0.712857	0.712846	0.711437	0.724667	0.724088	0.704974	0.713197
9	10.66	3.51	4.74	11.38	11.38	5.93	14.84	14.84	1.83	5.64
10	42.35	10.75	14.11	49.57	49.57	22.11	80.81	80.81	5.57	24.14
11	0.152	0.198	0.203	0.139	0.139	0.139	0.111	0.111	0.199	0.141
12	0.512121	0.512369	0.512858	0.512087	0.512094	0.512309	0.511736	0.51175	0.512816	0.512226
13	−10.0	−5.1	4.4	−10.6	−10.5	−6.3	−17.5	−17.2	3.6	−7.9
14	0.92	0.36	0.34	0.69	0.69	0.49	0.97	0.97	0.24	0.67
15	7.9	2.32	2.2	8.14	8.14	3.81	11.46	11.46	1.21	4.01
16	0.0165	0.022	0.0219	0.012	0.012	0.0183	0.012	0.012	0.0282	0.0237
17	0.282462	0.282683	0.282919	0.282396	0.282402	0.282694	0.282211	0.282203	0.282974	0.282588
18	−11.4	−3.6	4.7	−13.8	−13.5	−3.2	−20.3	−20.6	6.7	−7.0
19	0.86	0.23	0.23	0.56	0.56	0.44	2.21	2.21	0.15	0.69
20	5.4	1.15	0.61	3.93	3.93	3.04	36.92	36.92	0.22	5.95
21	13.03	4.26	4.23	15.90	15.90	4.61	30.31	30.31	0.45	7.14
22	4.2	3.4	3.4	2.2	2.2	6.0	4.6	4.6	20.9	6.2
23	27.1	17.6	9.4	15.9	15.9	43.2	79.9	79.9	31.7	54.9
24	17.817	17.793	18.327	17.277	17.290	17.727	17.539	17.537	17.867	17.885
25	15.68	15.637	15.602	15.592	15.588	15.622	15.632	15.631	15.597	15.664
26	38.633	38.464	38.186	38.15	38.151	38.989	39.241	39.219	38.146	39.267
27	0.71337	0.70758	0.70362	0.71146	0.71144	0.70975	0.71804	0.71746	0.70457	0.71114
28	0.511992	0.512201	0.512685	0.511969	0.511976	0.512191	0.511642	0.511656	0.512647	0.512106
29	−9.2	−5.2	4.3	−9.7	−9.5	−5.4	−16.1	−15.8	3.5	−7.0
30	0.282422	0.282630	0.282866	0.282367	0.282373	0.282650	0.282182	0.282174	0.282906	0.282530
31	−9.9	−2.6	5.8	−11.9	−11.7	−1.9	−18.4	−18.7	7.2	−6.1
32	17.73	17.72	18.26	17.23	17.25	17.60	17.45	17.44	17.44	17.76
33	15.68	15.63	15.60	15.59	15.59	15.62	15.63	15.63	15.58	15.66
34	38.46	38.35	38.13	38.05	38.05	38.71	38.73	38.70	37.94	38.91
35										
36										
37										
38										
39										
40										
41										
42										
43										
44										
45										
46										
47										
48										
49										